Int. J. Electrochem. Sci., 3 (**2008**) 819 - 853

International Journal of ELECTROCHEMICAL SCIENCE
www.electrochemsci.org

Carbon Nanotube Based Modified Electrode Biosensors. Part 1.Electrochemical Studies of the Flavin Group Redox Kinetics at SWCNT/Glucose Oxidase Composite Modified Electrodes.

Michael E.G. Lyons[*]*, and Gareth P. Keeley*

Physical and Materials Electrochemistry Laboratory, School of Chemistry, University of Dublin, Trinity College, Dublin 2, Ireland.
[*]E-mail: melyons@tcd.ie

Received: 5 May 2008 / *Accepted:* 23 May 2008 / *Online published:* 30 June 2008

The redox behaviour of glucose oxidase adsorbed on glassy carbon electrodes which have been modified with a dispersed mesh of single wall carbon nanotubes is probed both qualitatively and quantitatively using cyclic voltammetry and potential step chronoamperometry. We have shown that potential step chronoamperometry is the method of choice when conducting kinetic measurements for three reasons. First, the analytical theory is simple to implement. Second, the effects of double layer charging are readily recognized and accounted for in subsequent data analysis. Third the effects of kinetic dispersion are readily identified and taken into consideration in data analysis.

Keywords: Protein film voltammetry, Glucose Oxidase electrochemistry, Carbon nanotube modified electrode, Chronoamperometry of surface immobilized systems, Gaussian kinetics.

1. INTRODUCTION

Since the discovery of carbon nanotubes (CNTs) by Iijima in 1991 [1], there has been an explosion of research into the physical and chemical properties of these fascinating structures. CNTs can be described as sp^2 carbon atoms arranged in graphitic sheets seamlessly wrapped into cylinders and capped by fullerene-like hemispheres. Single-walled carbon nanotubes (SWCNTs) display excellent chemical stability, good mechanical strength and a range of electrical conductivity. They are at least ten times stronger than steel, around six times lighter and, depending on their chirality and diameter, can behave as metals, semiconductors or insulators. In a typical sample, around one third can be thought of as metallic. Due to their high surface energies, SWCNTs are usually found in bundles composed of tens to hundreds of tubes in parallel and in contact with each other. Multi-walled carbon

nanotubes (MWCNTs) comprise of several layers of graphitic cylinders, which are concentrically nested like the rings of a tree trunk. They are regarded entirely as metallic conductors, which in some respects makes them more suitable for electrochemical applications. However, SWCNTs are more well-defined systems, making their electrochemical properties easier to understand. The electrochemical properties of both multi (MWCNT) and single walled (SWCNT) carbon nanotubes have not been extensively examined to date, although these materials should serve as excellent candidates for nanoelectrodes and platforms for nanoelectrochemical cells and amperometric biosensor devices [2,3].

Electron transfer in biological systems is one of the leading areas in the biochemical and biophysical sciences [4], and in the past few years there has been considerable interest in the direct electron transfer between redox proteins and electrode surfaces. The direct electrochemistry of the heme proteins and flavo enzymes has been widely investigated since the 1970s. Glucose oxidase (GOx) is a large, dimeric protein with a formula weight of 160 kDa. It catalyses the oxidation of β-D-glucose to δ-D-gluconolactone. Glucose oxidase contains one tightly-bound flavin adenine dinucleotide (FAD) unit per monomer. These redox-active prosthetic groups are not covalently bound and may be released from the protein during denaturation. However, in the absence of mediating small molecules, well-defined electrochemical behaviour of flavoprotein-oxidase systems such as GOx is rendered extremely difficult because the flavin adenine dinucleotide (FAD) prosthetic group is embedded deep within the protein structure.

Various immobilization strategies [5,6] have been adopted to fabricate enzyme electrodes for biosensor applications. These strategies have exhibited varying degrees of success and in many cases electron transfer mediators have to be used to facilitate electronic communication between the active site of the protein and the underlying electrode. However the potential at which an amperometric enzyme biosensor is operated depends upon the redox potential of the mediator used rather than that exhibited by the active site of the redox enzyme. Usually the difference in magnitude between the latter potentials is significant (ca. 0.3 - 0.5 V) a factor which acts against successful biosensor operation, since the more positive the operating potential, the greater is the tendency for the sensor to respond to oxidizable substances present in the sample other than the target substrate.

Clearly, the best strategy for successful enzyme biosensor fabrication is to devise a configuration by which electrons can directly transfer from the redox center of the enzyme to the underlying electrode. This has been accomplished in recent years using the idea of molecular wiring. Hence the enzyme can be modified with electron relays, through modification of the peripheral oligiosaccharide with relay species pendant on the termini of flexible spacer chains, and indeed through relays in electron conducting hydrogels within which enzymes are covalently bound.

The similarity in length scales between nanotubes and redox enzymes suggest the presence of interactions that may be favourable for biosensor electrode applications [7]. The strategy of physical adsorption or covalent immobilization of large biomolecules onto the surface of immobilized carbon nanotubes may well represent an exciting pathway through which direct electrical communication between electrodes and the active site of redox-active enzymes can be achieved. It is hoped that the electrocatalytic properties of carbon nanotubes will have applications in the development of enzyme biosensors without mediators. Indeed recent work reported in the literature suggests that this objective

might well be feasible. For instance recent work [8,9] has indicated that the chemical modification of electrode surfaces with carbon nanotubes has enhanced the activity of electrode surfaces with respect to the catalysis of biologically active species such as hydrogen peroxide, dopamine and NADH.. Furthermore, multiwalled carbon nanotubes have exhibited good electronic communication with redox proteins where not only the redox center is close to the protein surface such as in Cytochrome c , azurin and horseradish peroxidase, but also when it is embedded deep within the glycoprotein such as is found with glucose oxidase [10,11]. In many situations the nanotubes are dispersed on the surface of a support electrode to form a randomly dispersed array of high surface area, or else incorporated as a dispersion within a matrix to form a thin film. In a notable paper described recently [12] direct electrical wiring of glucose oxidase to a support electrode has been achieved using well ordered arrays of carbon nanotubes .

This is the first in a series of three papers dealing with carbon nanotube based chemically modified electrodes. In the present paper we focus on an examination of the electrochemical behaviour of GOx adsorbed on electrode surfaces modified with SWCNT meshs. We apply the techniques of linear potential sweep voltammetry and cyclic voltammetry to quantify the redox kinetics of the FAD/$FADH_2$ transformation. In particular, we utilise a Gaussian model [13] for investigation of the kinetics of the FAD/$FADH_2$ transition, which we believe is more appropriate than any others that have been previously applied, to analyse the kinetics of surface-immobilised redox enzymes to date. We indicate how this Gaussian model can be applied to modify the theory of Laviron [19] which is often used to describe the current response to a linear potential sweep exhibited by a surface immobilized redox couple. The second paper in the series will concern the catalytic behaviour of these composite modified electrodes with respect to the oxidation of glucose under amperometric conditions and at various applied potentials. We will argue that amperometric glucose detection is possible at very low potential and examine possible mechanisms by which this low potential (and hence desirable) detection is achieved. The third paper will examine the catalytic activity of electrodes modified with SWCNT meshes with respect to the oxidation and reduction of molecules of biological significance and discuss issues relating to the mechanism of catalysis at SWCNT surfaces.

2. EXPERIMENTAL

2.1 Materials

Glucose oxidase (GOx, Type VII, from *Aspergillus Niger*, 198 kU/g or 221 kU/g), Nafion (~5% in a mixture of lower aliphatic alcohols and water), potassium ferricyanide and potassium chloride were purchased from Sigma and used as received. Single-walled carbon nanotubes (SWCNTs), HIPCO type, were purchased from Carbon Nanotechnologies Inc., Houston, Texas, USA, and used as supplied. Using thermo-gravimetric analysis, we showed that the iron content of these nanotubes was around 12 wt %. β-D-glucose was purchased from ICN Biomedicals, Inc. Glucose stock solutions were stored overnight at room temperature before use to allow equilibration of anomers. Hydrogen peroxide (30 wt %) was purchased from Sigma-Alrich. This was freshly diluted to the appropriate concentration each day and used immediately. Oxygen-saturated solutions were made by purging with high-purity O_2

for at least ten minutes. The concentration of saturated aqueous oxygen solutions at room temperature is roughly 1.2mM [7]. All solutions were prepared with water (18.2 MΩcm) from an Elix® Millipore system..

All other chemicals were of analytical grade. All solutions were prepared using millipore water. A standard 50 mM pH 7 phosphate buffer was purchased from Sigma and employed as supporting electrolyte except in the pH studies (Section 3.1.2). For studies in which pH had to be varied, buffers of various pH values were prepared by dissolving different ratios of monosodium dihydrogen phosphate dihydrate ($NaH_2PO_4.2H_2O$) and disodium hydrogen phosphate dodecahydrate ($Na_2HPO_4.12H_2O$) in millipore water. For these experiments acetate, phosphate and ethanolamine buffers of various pH values were used.

2.2. Electrode Modification

In this work the surfaces of the working electrodes (either gold or glassy carbon) were renewed by carrying out a standard polishing procedure prior to experiments in order to yield a reproducible surface morphology free from adsorbed impurities, as verified by cyclic voltammetry. The polishing kit used was purchased from IJ Cambria and contained a range of alumina polishing powders (1.0, 0.3 and 0.05 microns) and a range of polishing pads made from different materials (Nylon and Microcloth). Initially, electrodes were polished by a 'figure-of-eight' motion on Nylon pads covered with a paste of 1.0 micron alumina in millipore water (see Figure xxxx). After thorough rinsing with the latter, they were polished in the same way using 0.3 micron alumina and Nylon pads. Finally, after more rinsing, they were polished once more, using 0.05 micron alumina and Microcloth pads. When carrying out measurements using bare glassy carbon, the electrodes were placed immediately in the electrochemical cell. When further modification was required, they were blown dry using a stream of nitrogen and promptly modified.

A suspension of single-walled carbon nanotubes was prepared by adding SWCNTs (1 mg) to either dimethyl formamide (DMF) (10 cm^3) or *N*-methyl-2-pyrrolidone (NMP) (10 cm^3) and sonicating for five minutes. This suspension (1 μL) was cast on inverted gold and glassy carbon macroelectrodes and the organic solvent was evaporated using a fan heater at 40 °C for approximately fifteen minutes. The electrode was rinsed sequentially with water and working electrolyte before all experiments. This resulted in the deposition of roughly 0.4 μg of nanotubes on the electrode surface. Tubes were often seen to 'spill over' onto the Kel-F casing so this value of 0.4 μg may be interpreted as a maximum. The films were clearly visible to the naked eye. In our experience, 13 μg cm^{-2} (0.4 μg on an electrode with geometric area 0.03 cm^2) gave an optimum electrochemical performance. Greater nanotube coverages sometimes resulted in evidence of passivation of the electrode surface, possibly due to the poor conductivity across the walls of the tubes compared to along the walls. The GC/SWCNT electrodes were rinsed sequentially with millipore water and working electrolyte before experiments.

Solutions of glucose oxidase were prepared by adding GOx (3 mg) to a 50 mM pH 7 phosphate buffer solution (1 cm^3). The enzyme was physically adsorbed on electrode surfaces by drop-coating these solutions (10 μL) and allowing the solvent to evaporate at room temperature for approximately 2.5 hours. When heat was used no evidence of enzyme activity was observed, most

likely due to denaturation. Finally, Nafion (1 μL) was cast and allowed to dry at room temperature. The resulting film covered the gold and the surrounding epoxy encasement or the glassy carbon and surrounding Kel-F emplacement, and was clearly visible to the naked eye. Finally, the modified electrode was rinsed with buffer solution and, with residual buffer still covering the electrode surface, transferred immediately to the cell.

An AFM image recorded for the nanotube dispersion is presented in figure 1(a). The random dispersed nature of the assembly is apparent from the figure.

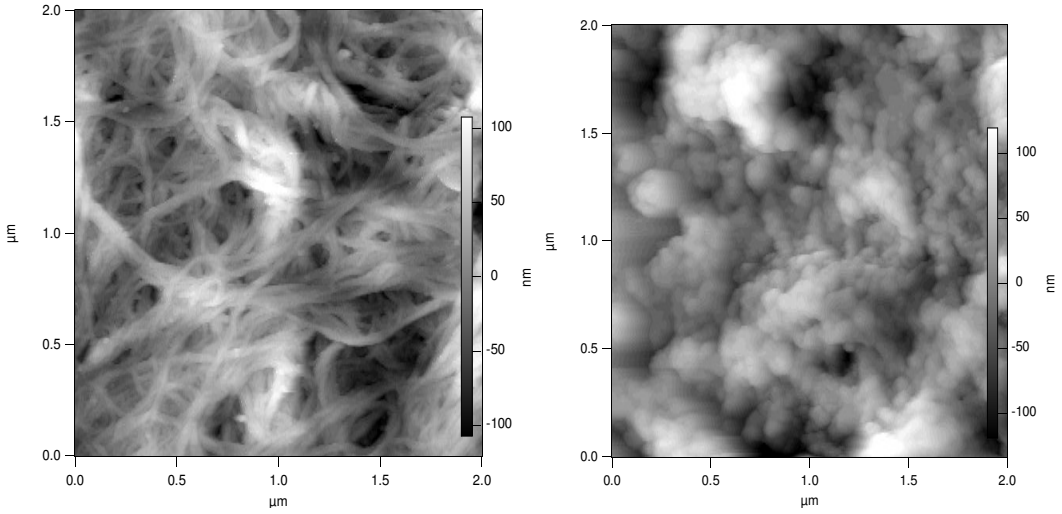

Figure 1. (a) AFM image recorded for ensemble of SWCNT dispersed randomly on a gold surface. (b) AFM image recorded for a SWCNT assembly dispersed randomly on a gold surface on which glucose oxidase was adsorbed for a 2.5 hr period at room temperature.

2.3. Apparatus

A CH Instruments Model 440 potentiostat was used to perform all electrochemical experiments, along with a conventional three-electrode cell. Platinum wire and Ag/AgCl were used as counter and reference electrodes, respectively. Buffers were purged with high-purity nitrogen for at least twenty minutes prior to experiments and a nitrogen environment was then maintained over solutions in the cell throughout all scans. All work was performed at room temperature (20 ± 3 °C).

3. RESULTS AND DISCUSSION

3.1. General electrochemical properties of SWCNT/GOx-modified electrodes

In this section of the paper we concentrate on examining the general electrochemical characteristics of glucose oxidase which has been adsorbed on an assembly of single walled carbon nanotubes randomly dispersed both on gold and glassy carbon support electrode surfaces. A typical AFM image recorded for a nanotube assembly (dispersed in this case on a gold surface) on which glucose oxidase has been adsorbed is outlined in figure 1(b). It is clear from the latter image that the

enzyme fills much of the void space between the nanotube bundles. Hence we expect that the enzyme loading should be at a level to ensure good catalytic activity. It is prudent to note, however, that this arrangement may be different from what prevails during an electrochemical measurement, when Nafion is binding the system to the underlying glassy carbon electrode, a current is passing through the assembly and a double layer has been set up. In our experiments the support electrodes were initially modified with an assembly of SWCNT as outlined previously. The SWCNT modified support electrode was then thoroughly washed with water and immersed in a 16 mg mL^{-1} GOx in phosphate buffer solution (0.05 M, KH_2PO_4 + Na_2HPO_4, pH 7) at 20^0C for ca. 2.5 hours. Adsorption of glucose oxidase onto the SWCNT occurs within this timescale. In some experiments the enzyme SWCNT composite electrode was further modified by depositing a thin layer of soluble nafion via drop coating. The resulting enzyme modified electrodes were then subjected to electrochemical analysis (largely cyclic voltammetry and potential step chronoamperometry) in phosphate buffer solution.

The electrochemical response of the latter enzyme modified SWCNT modified electrode was determined using cyclic voltammetry. The voltammograms presented in Figure 2 were obtained using a bare, SWCNT-modified and SWCNT/GOx and SWCNT/GOx/Nafion-modified glassy carbon working electrodes in a 50 mM phosphate buffer (pH 7). As can be seen, while a bare GC electrode exhibits a virtually flat and featureless voltammetric response, a pair of well-defined redox peaks was observed at the both the SWCNT/GOX and SWCNT/GOx/Nafion-modified electrode. The observed peaks are characteristic of those representing the redox behaviour of an adsorbed species, in this case that of the flavin adenine dinucleotide FAD. The peaks are reasonably symmetrical and exhibit the characteristic bell shape expected for adsorbed redox species [19]. The absence of any peaks on the SWCNT-modified GC voltammogram suggests that the voltammetric response observed with the latter is essentially capacitive in the absence of any redox active substrates present in the electrolyte solution.

For the voltammetric response of the SWCNT/GOx/Nafion composite electrode at a sweep rate of 100 mVs^{-1}, the cathodic peak potential (E_{pc}) is -417 mV vs. Ag/AgCl and the peak separation (ΔE_p) is 41 mV. The surface coverage of adsorbed redox enzyme can be calculated by integrating the charge Q under the voltammetric peak using the formula: $\Gamma = Q/nFA$ where A denotes the geometric electrode area , n denotes the number of electrons transferred in the redox process (2 in the present case) and F is the Faraday constant. We estimate that Γ = 1.7 nmol cm^{-2} for the Nafion coated SWCNT/GOx composite electrode. The corresponding data set for the SWCNT/GOx composite without the Nafion overlayer is a cathodic peak potential (E_{pc})of -449 mV vs. Ag/AgCl and a peak separation (ΔE_p) of 24 mV. It is difficult to estimate the surface coverage for the latter system since the resolution between Faradaic and capacitive processes is poor. Consequently we do not provide a numerical estimate for this quantity but merely note that it is certainly less that that recorded for the Nafion coated system. Furthermore the redox peaks become indiscernible when the modified electrode is subjected to a repetitive potential cycling regime in phosphate buffer solution.

In figure 3 we compare the voltammetric response recorded at a SWCNT modified glassy carbon electrode with a SWCNT/GOx modified glassy carbon electrode but without the addition of a Nafion overcoating. Here we note that evidence of flavin group redox activity is to be found for the SWCNT/GOx system, but in general the redox peaks are somewhat ill defined. Comparing figure 2 and figure 3 we see that the addition of Nafion clearly enhances the dispersion of the Nanotube

bundles on the support electrode surface which may then enhance the effectiveness of the nanotube wiring to the embedded flavin active site of the immobilized glucose oxidase, and hence result in more effective charge transfer kinetics and potential directed turnover of the flavin group.

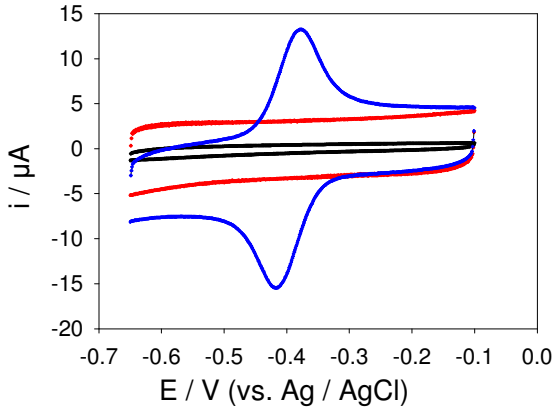

Figure 2. Cyclic voltammograms recorded at a bare (black), SWCNT-modified (red) and SWCNT/GOx /Nafion-modified (blue) glassy carbon working electrode. The electrolyte used in these experiments was a 50 mM phosphate buffer (pH 7) and the scan rate employed was 100 mV s^{-1} .

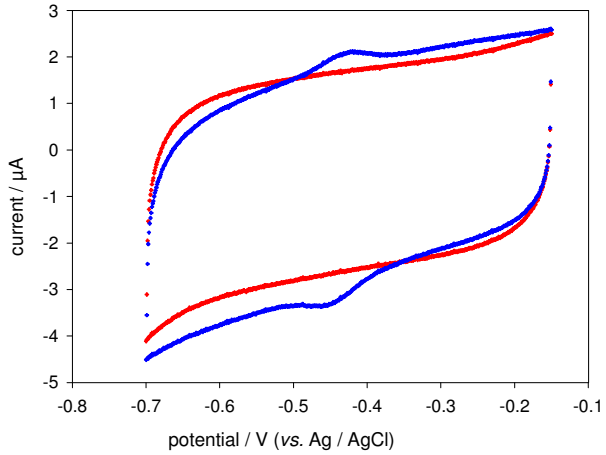

Figure 3. Cyclic voltammetric response of a SWCNT modified GC electrode (red curve) and a SWCNT/GOx modified GC electrode (blue curve). Sweep rate, 50 mV/s. Phosphate buffer pH 7.

In Figure 4 the protein film voltammetry of GOx adsorbed on unmodified glassy carbon surfaces and on SWCNT modified glassy carbon surfaces is compared. Again we see evidence of enzyme redox activity on glassy carbon in the absence of NTs but the peaks are not sufficiently defined to be useful for quantitative analysis purposes. With the nanotube-modified electrode, the area beneath the enzyme peaks is relatively large, indicating a far larger quantity of adsorbed, active enzyme.

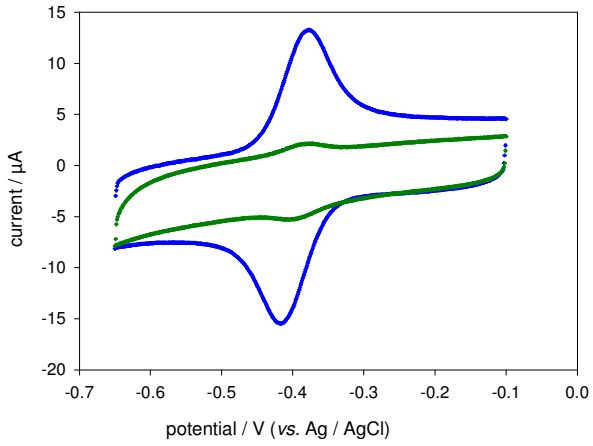

Figure 4. Cyclic voltammetric response of a GOx/Nafion modified glassy carbon electrode (green) and a SWCNT/GOx/Nafion modified glassy carbon electrode (blue). The protein film voltammetry was recorded in 50 mM phosphate buffer solution pH 7 at a sweep rate of 100 mV s^{-1}.

It is useful at this stage to comment on the nature of the interactions which result in enzyme immobilisation on the nanotube film, as our experiments presented in figure 3 and 4 indicate that addition of a Nafion overcoating to the nanotube/GOx composite modified electrode enhances the redox activity of the latter and that the nanotube modified electrode is clearly superior to glassy carbon as an enzyme immobilisation platform. Wang *et al.* [8] have reported that glucose oxidase adsorbs preferentially to edge-plane sites on nanotubes. It has been established that such sites contain a significant amount of oxygenated functionalities. These groups are formed *via* the rupturing of carbon-carbon bonds at the nanotube ends and at defect sites which may occur on the side-walls. They render hydrophilicity and ionic character to the nanotubes and we believe that they are responsible for the 'nesting' of the protein on the nanotube film. The nanotubes and enzyme molecules are of similar dimensions , which facilitates the adsorption of glucose oxidase without significant loss of its biocayalytic shape, form or function. We suggest that nanotubes can pierce the glycoprotein shell and gain access to the prosthetic group such that the electron tunneling distance is minimized. Such access is not generally possible with conventional 'smooth' electrodes, and significant unfolding of the protein shell can occur, resulting in the loss of biochemical activity.

Furthermore Wang and co-workers [8] have reported that SWCNT are readily solubilized in Nafion solutions made from ethanol or aqueous phosphate buffer. TEM images clearly indicate individual SWCNT ropes when dispersed in the latter media. This is in contrast to the high density intertwined aggregates found when SWCNT are dispersed in organic solvents such as chloroform. The structure of Nafion in solution may be viewed as a fluorocarbon backbone with protruding polar sulfonate SO_3^- groups. Hence it is similar in nature to other polymers which have been used to wrap and solubilise CNT material. According to Smalley and co-workers [20] the wrapping of nanotubes by water soluble polymers such as Nafion is a general phenomenon driven by a thermodynamic impetus to eliminate the hydrophobic interface between the tubes and the aqueous medium, thereby reducing

the density of the tangled and rather dense tube assembly on the electrode surface. This may well increase the permeability of the void space between the tubes to increased quantities of electrolyte ions which will result in a change in the interfacial potential distribution and hence on the voltammetric response [21].

Ideally ΔE_p should be zero for surface immobilized redox systems, [19,22] . The non zero ΔE_p value observed in both cases above may be attributed to the presence of a potential difference between the electrode and the site of electron transfer (the flavin redox group) [23]. Such a difference would be attributed to the surrounding protein sheath acting as a dielectric layer. The presence of Nafion, while enhancing the discrimination between currents resulting from the surface redox reaction and that arising from the capacitive background contribution, may well result in a larger potential drop in the interface region. The prominent background current is a consequence of the large, catalytically active surface area of the modified electrode [24,25].

The most important result obtained from the voltammetry data is the clear set of redox peaks obtained. We contend that the latter are due directly to the direct electron transfer between the flavin prosthetic group embedded within the protein sheath and the underlying carbon nanotube strand. Hence we propose that the GOx molecules are adsorbed in a reasonably pristine configuration where the tunneling distance for electron transfer between the flavin sites and the nanotube strand is not too large hence making the transition probability for electron transfer favourable. It is important to note that the carbon nanotube and the enzyme molecule share a similar length scale and so the enzyme is able to adsorb on the nanotube sidewall without losing its biologically active shape, form and function. Indeed Baughman and co-workers [7] have introduced the striking analogy of piercing a balloon with a long sharp needle such that the balloon does not burst. Instead by a gentle twisting action the needle can be made to enter the balloon without catastrophe. Similarly it has been proposed [7] that some number of nanoscale 'dendrites' of CNT project outwards from the surface of a strand and act like bundled ultramicroelectrodes that are able to pierce the glycoprotein shell of glucose oxidase and gain access to the flavin prosthetic group such that the electron tunnelling distance is minimized and consequently electron transfer probability optimized. This degree of nanoscale electronic wiring and intimate access is not generally afforded with traditional smooth electrodes.

It could, of course, be suggested that the GOx species loses its flavin group on adsorption, and one may query whether the flavin moiety dissociates from the surrounding glycoprotein sheath when glucose oxidase is adsorbed on the surface of the nanotube. The flavin (either present in the solution or adsorbed on the nanotube surface) could then function as an inefficient redox mediator. In a recent paper Baughman and co-workers [7] examined the redox behaviour of both the free flavin molecule in the adsorbed state and when it is bound within glucose oxidase at single walled carbon nanotube modified electrodes using potential sweep voltammetry. The standard potential of the $FAD/FADH_2$ transition for both forms of flavin environment were similar, typically – 0.45 V vs Ag/AgCl (in good agreement with our data (E^0 = - 0.396 V see figure 2)) and so it is difficult to differentiate between adsorbed flavin and adsorbed protein bound flavin. Both forms give rise to characteristic bell shaped responses when subjected to a linear potential sweep. However if the flavin is free in solution then the voltammetric response observed should be quite different. A characteristic diffusive response is expected in the voltammogram. This is not observed in our work (again refer to fig.2). Furthermore if

the voltammetric response observed in figure 2 arose from ET activity associated with adsorbed flavin molecules then one would expect that the voltammogram would be considerably distorted because of the fact that the electron would have to tunnel through a blocking layer of adsorbed holo-enzyme molecules which would also be present on the nanotube surface [26]. This distortion in the voltammetric profile is not observed.

The denaturation of glucose oxidase on a metal electrode surface has been experimentally examined using ellipsometry by Bockris and co-workers [26]. In this work two orientations of the enzyme molecule (shaped as a prolate ellipsoid with a major axis of 140 Å and minor axis of 50 Å) on the surface were observed: the major axis could be perpendicular to the surface (labelled the standing position) or parallel to the surface (termed the lying position). It was determined that above a certain coverage enzymes in the standing position were not stable and undergo a transition to the lying position due to increasing intermolecular interaction. In the lying position the enzyme/substrate contact area is large and a gradual unfolding of the glycoprotein sheath occurs brought about largely by significant electrostrictive forces operating in the double layer region. The catalytic function of the enzyme is adversely effected because of this and eventually catalytic activity is lost. Hence a key determining factor in determining enzyme structural stability is the manner in which the enzyme is orientated with respect to the support electrode surface. Finally, as will be discussed in detail in part 2 of this series of papers, we have noted in our experiments that catalytic activity with respect to glucose oxidation is observed only when a soluble mediator such as oxygen or ferrocene monocarboxylic acid is present in the solution. Catalytic glucose oxidation does not occur if adsorbed glucose oxidase is only present. The homogeneous mediator is required to ensure efficient charge shuttling between the flavin active site buried deep within the protein sheath and the underlying carbon nanotube sidewall. Oxygen and ferrocene molecules are of the correct size to enter the glycoprotein sheath effectively and interact with the flavin group.

The influence of experimental timescale manifested as scan rate on the system was investigated within the range of 0.005 to 5.0 Vs^{-1} for gold and 0.002 to 13.0 Vs^{-1} for glassy carbon. Figure 5 shows a comparison between voltammograms obtained at five different scan rates when a gold support electrode is used. A similar type of response is obtained when glassy carbon is the substrate.. In both situations it was found that the peak currents exhibited a linear relationship with the sweep rate, a feature which is characteristic of surface-bound redox processes as outlined in the analytic theory proposed by Laviron [19,22]. Figure 5(b) shows the variation of i_{pc} with ν for lower scan rates. The linearity was reasonably evident over the entire range of sweep rates studied. However studies conducted over a more extended sweep rate range indicated a breakdown in the direct proportionality between peak current and sweep rate. A deviation from strict linearity was observed and peak currents were found to be smaller than predicted assuming the maintenance of strict linearity. This observation may well be due to potential drop effects across the adsorbed enzyme layer.

It is important to examine the extent to which GOx/SWCNT composite modified electrodes may be fabricated in a reproducible manner. To this end four GC/SWCNT/GOx/Nafion electrodes were prepared independently and protein film voltammetry was carried out at a number of different sweep rates using phosphate buffer (pH 7.0) as electrolyte. The average reduction peak current was 5.94 μA at 50 mVs^{-1},a value much larger than the 0.75 μA reported by Liang and Zhoubin [27] using a

SWCNT/GOx-modified gold working electrode at 100 mVs^{-1}. However, at around 20%, the standard deviation of these currents was significant. This is hardly surprising though, given the inherently random nature of the deposition process. We note that the nanotube-modified electrodes are not endowed with reproducible active surface areas. Even if they were, finding a way to control the orientation of the enzyme on the nanotube array would represent a major challenge. It should be pointed out though that Liang and Zhoubin [27] report a deviation of only 6.5 % using a similar electrode preparation procedure. The average value for the ratio of anodic to cathodic peak current was found to be very close to unity (~0.98), suggesting a quasi-reversible redox process [27]. Standard redox potentials and peak separations were found to exhibit impressive reproducibility, as shown in Table 1.

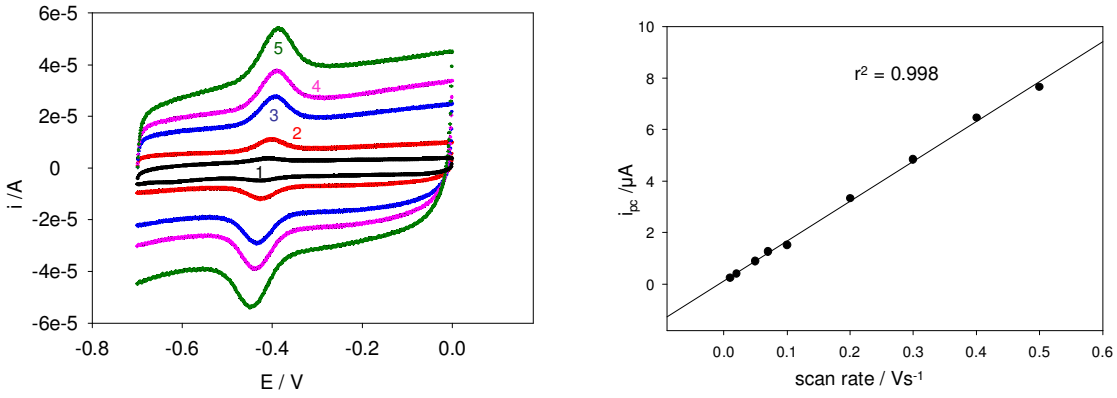

Figure 5. (a) Cyclic voltammograms obtained using a SWCNT/GOx-modified Au working electrode. The electrolyte used was a 50 mM PBS (pH 7). The scan rates shown are (1) 0.1, (2) 0.3, (3) 0.8, (4) 1.1 and (5) 1.5 Vs^{-1}. (b) The variation of cathodic peak current with scan rate using a SWCNT/GOx-modified Au working electrode. The electrolyte used was a 50 mM PBS (pH 7).

The E^0 values listed are average values over the range of scan rates studied, with appropriate standard deviations, showing that the standard redox potential of the system is independent of sweep rate over this range. Ideally, a fully reversible system involving no solution reactants, peak separations should be zero [25]. The discrepancy may be due to a potential difference between the electrode and the site of activation (the flavin group). Such a difference would be attributed to the protein acting as a dielectric layer, and if true, indicate that enzyme does not unfold significantly on the nanotubes. These E^0 values are significantly less negative than the -659 mV *vs.* Ag / AgCl reported by Zhao *et al.* [15] for GOx immobilised at a carbon nanotube powder microelectrode (CNTPME). They are, however, similar to those reported by other workers studying the direct electrochemistry of glucose oxidase using various immobilisation methods. The prominent background currents observed are a consequence of the large, catalytically active surface area of the modified electrode. The formal

potential of the FAD / $FADH_2$ redox couple is -0.43 V *vs.* Ag / AgCl [23], so we see that our E^0 values agree strongly with that of the native molecule.

Table 1. Summary of redox potential and peak separation data obtained for four independently-prepared GC/SWCNT/GOx/Nafion electrodes.

Electrode	E^0 / mV	ΔE_p @ 50 mVs^{-1}
1	-442 ± 2	17 mV
2	-439 ± 1	24 mV
3	-442 ± 1	19 mV
4	-443 ± 2	14 mV

The stability of the electrochemical response shown by the GC/SWCNT/GOx/Nafion system was probed by carrying out one hundred successive scans at 50 mVs^{-1} in phosphate buffer (pH 7.0). Reduction peak currents were normalised with respect to the initial value and plotted against scan number, as shown in Figure 6. These peak currents were found to drop sharply at first and then more steadily as the number of cycles increased. After one hundred cycles, the signal had decayed to around 45 % of its initial value but remained well-defined, as shown in Figure 6(b).

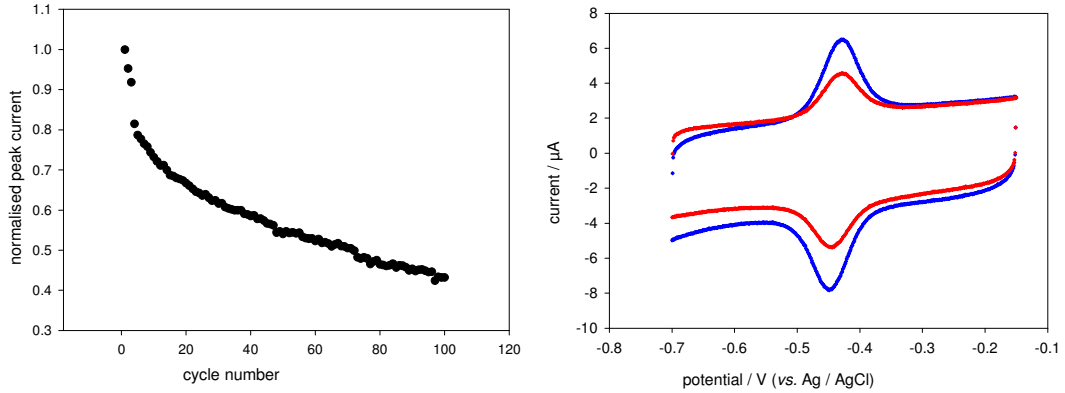

Figure 6. (a) Variation of normalized peak current with cycle number during repetitive potential cycling of GC/SWCNT/GOx/Nafion modified electrode in phosphate buffer solution. (b) Schematic representation of voltammograms recorded at initial cycle, N = 1 (blue curve) and final cycle N = 100 (red curve).

The storage stability of the GC/SWCNT/GOx/Nafion system was investigated by storing an electrode in buffer and scanning in buffer every day for four days. By the third day, peak currents were found to have decreased to less than 10 % of their initial values. As a result, it was decided that for fundamental measurements on the redox, kinetic and catalytic behaviour of the system, fresh electrodes should be prepared daily.

In another series of experiments we have examined the potential of the modified electrode preparation procedure with regard to the reproducibility of enzyme loading. The results are outlined in Table 2 below.

Table 2. Enzyme surface coverages for four independently prepared GC/SWCNT/GOx/Nafion modified electrodes.

Electrode	Area of GC/NT (cm^2)	Moles of active GOx	Γ ($pmolcm^{-2}$)
1	0.0880	1.43×10^{-11}	162
2	0.0910	0.823×10^{-11}	90.4
3	0.105	2.71×10^{-11}	258
4	0.107	1.49×10^{-11}	139

It is clear from these results that the enzyme surface coverage varies over a reasonable wide range typically 90-260 pmol cm^{-2}. These coverages are all significantly larger than corresponding values quoted in the literature. For instance Liang and Zhuobin [27] quote a value of enzyme surface coverage of 52 pmol cm^{-2} for a Au/SWCNT/GOx modified electrode in phosphate buffer solution. in contrast, Wang and Thai [28] report a much lower coverage of 3 pmol cm^{-2} determined at edge plane highly ordered pyrolytic graphite electrodes on which glucose oxidase is adsorbed. Gooding and co-workers [29] reported enzyme surface coverages of close to 1 pmol cm^{-2} at Au/SAM/GOx modified electrodes, and Zhao and co-workers [30] showed that larger enzyme coverages of close to 200 pmol cm^{-2} could be attained if the enzyme was immobilized within a carbon nanotube loaded polymer modified electrode.

We conclude therefore that the nanotube assembly provides a matrix for the efficient immobilisation of a large loading of glucose oxidase and the Nafion binder/dispersal agent succeeds in preventing the loss of significant amounts of this enzyme to the solution during electrochemical experiments. However a major issue with respect to practical biosensor fabrication is the variability in the extent of surface coverage attained of active enzyme using the rather simple fabrication methodology adopted in this work.

3.2 The effect of solution pH on the surface redox behaviour of the FAD/$FADH_2$ couple.

The $FAD^+/FADH_2$ system involves the transfer of two electrons and an associated protonation/deprotonation equilibrium $FADH_2 - 2H^+ - 2e^- \rightarrow FAD^+$ as illustrated below in scheme 1. This implies that the redox behaviour exhibited by the flavin groups should depend on the pH of the environment. In figure 7(a) we present a number of voltammograms recorded in various buffer solutions of known pH. The solution pH values were as follows: 5.2 (acetate buffer), 5.9, 7.0, 8.0 (phosphate) and 8.9 (ethanolamine). As can be seen, the position of the peak potential of FAD depends

on solution pH. All changes in voltammetric peak potentials and currents with pH were reversible, that is, the same voltammogram can be obtained if the electrode is transferred from a solution with a different pH value back to its original solution.

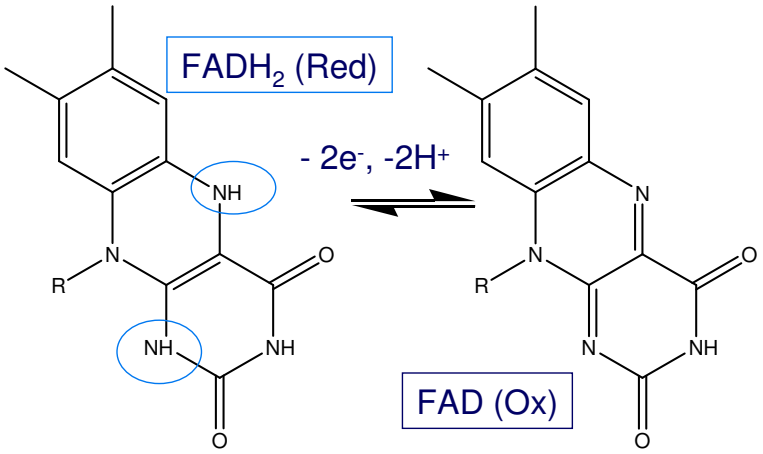

Scheme 1.

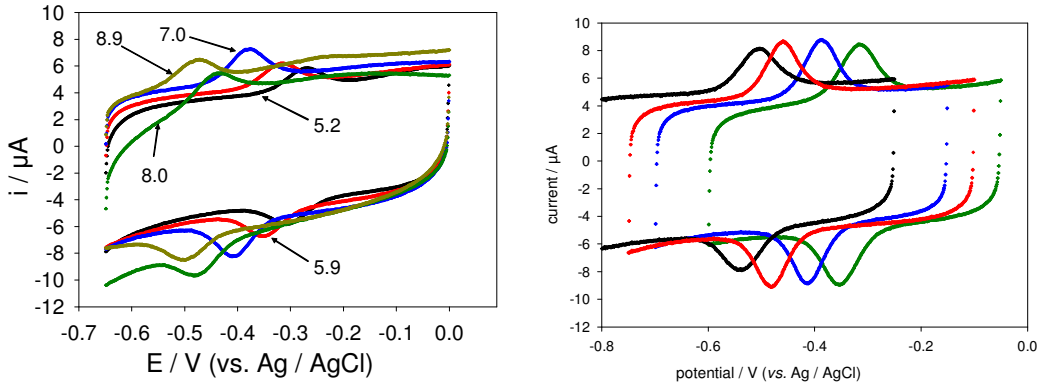

Figure 7. (a) Voltammogams obtained using a SWCNT/GOx/Nafion-modified gold working electrode in buffers of various pH values. The scan rate employed in each case was 100 mVs^{-1}. (b) Voltammograms obtained using a GC/SWCNT/GOx/Nafion electrode in 50 mM phosphate buffers of pH (from left to right) 8.6, 7.5, 6.3 and 5.1. The sweep rate employed in each case was 50 mVs^{-1}.

Within the pH range studied, the reduction peak potential was observed to shift cathodically with increasing pH value, with a slope of 56 mV per decade change of H^+ ion concentration, as shown in Figure 8(a). This result is in good agreement with the theoretical value of 59 mV per decade change of $[H^+]$ for a reversible, two-proton/ two-electron process at 22 °C [16], calculated using the Nernst

equation, and also with previous data published by Liang and Zhuobin [27] for adsorbed glucose oxidase on a SWCNT-modified gold electrode (48 mV/decade). The experiment was repeated for modified electrodes using glassy carbon as a support platform (fig7(b)). Four independently-prepared electrodes were investigated at seven pH values. The standard potential and two peak potentials were all found to shift cathodically with increasing pH, as shown in Figure 8(b). Three such plots were drawn for each electrode. The average slope of the twelve lines was found to be -53 (± 2) mV/pHHence the pH studies confirm the stoichiometry of the FAD/$FADH_2$ surface redox reaction as presented in scheme 1 .

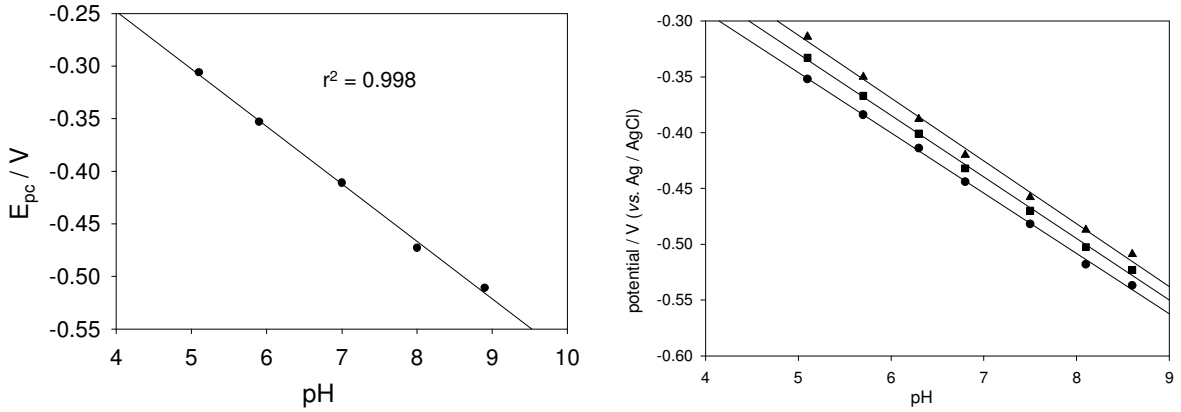

Figure 8. (a) The variation of the cathodic peak potential with pH obtained using a SWCNT/GOx/Nafion-modified gold working electrode in buffers of various pH values. The sweep rate employed in each case was 100 mVs^{-1}. (b) The variation of E_{pc} (●), E^0 (■) and E_{pa} (▲) with pH for a GC/SWCNT/GOx/Nafion electrode in 50 mM phosphate buffers of various pH values. The sweep rate employed here was 50 mV/s.

3.3 Quantifying the adsorbed flavin group kinetics: cyclic voltammetry and potential step chronoamperometry studies.

3.3.1. Potential sweep voltammetry.

Having established the details of the thermodynamics and stoichiometry of the adsorbed flavin group we now proceed to use electrochemical techniques to probe and extract quantitative information on the kinetics of the redox transition of the immobilized enzyme molecules. This analysis was accomplished using two techniques, linear potential sweep voltammetry and potential step chronoamperometry. We will contend that the latter method provides a more facile method of data analysis than the former, even though linear potential sweep voltammetry seems to be the method primarily adapted by workers in the field.

Linear potential sweep voltammetry may be used to extract kinetic parameters such as heterogeneous rate constants and transfer coefficients for surface immobilized redox reactions by examining the variation of voltammetric redox peak potential with experimental time scale (i.e. sweep

rate). Quantitative data analysis relies on a theoretical methodology originally developed by Laviron [19]. We will briefly summarize this analysis here.

The degree of kinetic reversibility exhibited by a surface redox reaction depends on the experimental timescale. It is expected that a surface redox reaction will exhibit reversible behaviour (manifested as a sweep rate invariant peak potential) when the sweep rate is small, and irreversible behaviour (indicated by a linear variation of peak potential with natural logarithm of sweep rate) when the sweep rate is large. This general expectation was confirmed in our experiments. When the scan rate is higher than 0.2 Vs^{-1}, it was observed that E_{pc} shifts negatively and E_{pa} shifts positively with increasing sweep rate. Figure 9 shows plots of anodic and cathodic peak potential as a function of the natural logarithm of the applied scan rate for a SWCNT/GOx/Nafion-modified gold (fig.9(a)) and glassy carbon (fig.9(b)) working electrodes. It is clear from both sets of experiments that the peak potentials are practically invariant with sweep rate when the latter is low, and in contrast for high sweep rates, peak potentials are proportional to ln ν.

For a surface-bound redox reaction involving redox active enzyme molecules adsorbed on surface immobilized SWCNT meshes, we can show that the following expression holds for the normalized current response for an oxidative potential sweep:

$$\Psi = \frac{i}{nF^2 A\Gamma_\Sigma \upsilon / RT} = m\left\{\left(\eta^\beta + \eta^{-(1-\beta)}\right)\mathrm{X}_R - \eta^{-(1-\beta)}\right\} \qquad (1)$$

where i denotes the current, Γ_Σ is the total redox group surface coverage (mol cm^{-2}), υ is the voltammetric sweep rate (V/s), A denotes the electrode area (cm^2) and m is a dimensionless parameter which relates the heterogeneous electron transfer rate constant to the experimental time scale and is given by $m = k_{ET}^0 / \sigma = k_{ET}^0 RT / F\upsilon$. Also in eqn.1 β represents the symmetry factor (typically ½) and $\eta = \exp[\xi]$, where the normalized potential is given by: $\xi = F(E - E^0)/RT$.

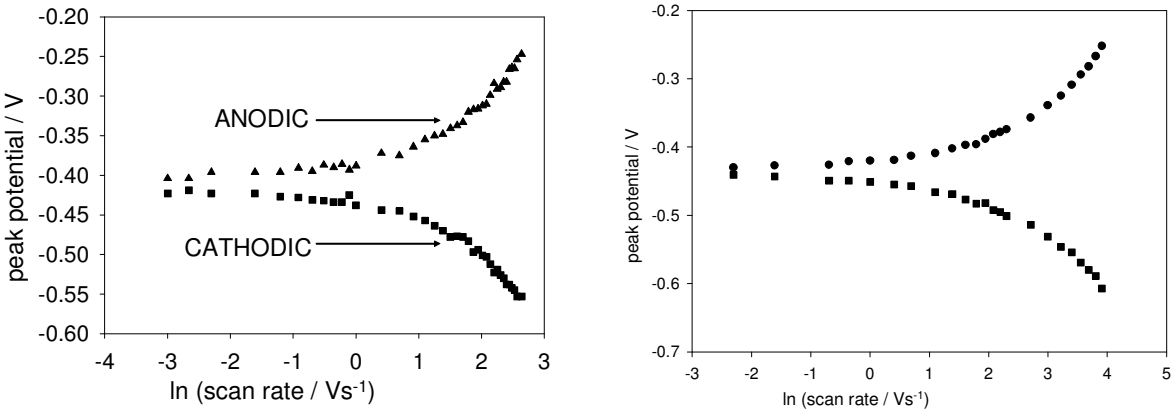

Figure 9. (a) Plots of anodic and cathodic peak potentials against the natural logarithm of scan rate for a SWCNT/GOx/Nafion-modified gold working electrode. The electrolyte used was a 50 mM phosphate buffer (pH 7). (b) Plots of anodic (●) and cathodic (■) peak potentials against natural logarithm of scan rate for a GC/SWCNT/GOx/Nafion electrode. Again, the electrolyte was a 50 mM PBS (pH 7.0).

Now the mole fraction X_R of reduced enzyme sites adsorbed on the SWCNT mesh is given by the solution to the following differential equation:

$$\frac{dX_R}{d\eta} + \frac{m}{\eta}\left(\eta^{\beta} + \eta^{-(1-\beta)}\right)X_R = \frac{m}{\eta}\eta^{-(1-\beta)} \tag{2}$$

This equation may be readily solved for suitable limiting values of the Laviron reversibility parameter m. First when the redox reaction is totally irreversible when $m \to 0$. Under these circumstances $\eta >> 1, \eta^{-1} << 1$ and eqn.2 reduces to:

$$\frac{dX_R}{d\eta} + m\eta^{-(1-\beta)}X_R = 0 \tag{3}$$

which can be readily integrated to yield

$$X_R \cong \exp\left[-\frac{m}{\beta}\eta^{\beta}\right] \tag{4}$$

and also for totally irreversible conditions we have $\eta^{\beta} >> \eta^{-(1-\beta)}$ and so the expression for the normalized current response presented in eqn.4 reduces to

$$\Psi \cong m\eta^{\beta}X_R = m\eta^{\beta}\exp\left[-\frac{m}{\beta}\eta^{\beta}\right] \tag{5}$$

This function exhibits a maximum or peak value designates as Ψ_p when $d\Psi/d\eta = 0$. We can readily show that under such conditions $\eta = \eta_p$ which is a maximum value, and

$$\frac{d\Psi}{d\eta} = \beta m\eta_p{}^{\beta-1}\exp\left[-\frac{m}{\beta}\eta_p{}^{\beta}\right] - m^2\eta_p{}^{\beta}\eta_p{}^{\beta-1}\exp\left[-\frac{m}{\beta}\eta_p{}^{\beta}\right] = 0 \tag{6}$$

Hence simplifying we obtain

$$\beta - m\eta_p^{\beta} = 0 \tag{7}$$

which simplifies to

$$\eta_p = \left(\frac{\beta}{m}\right)^{1/\beta} \tag{8}$$

Substituting eqn.8 into eqn. 5 we end up with the following simple result

$$\Psi_p = \frac{\beta}{e} \tag{9}$$

In terms of currents we obtain

$$i_p = \frac{\beta}{e}\left\{\frac{nF^2A\Gamma_{\Sigma}}{RT}\right\}\upsilon = S_{irrev}\upsilon \tag{10}$$

We also note that the normalized peak potential function is given by

$$\xi_{p,ox} = \ln\eta_{p,ox} = \frac{1}{\beta}\ln\left(\frac{\beta}{m}\right) = \frac{1}{\beta}\ln\beta + \frac{1}{\beta}\ln\frac{1}{m} \tag{11}$$

where we have written $\xi_p = \frac{F}{RT}(E_p - E^0) = \theta_p - \theta^0$ and we note that $\theta_p = \frac{FE_p}{RT}$, $\theta^0 = \frac{FE^0}{RT}$ represent normalized potentials. Hence we end up with a useful diagnostic expression for an irreversible surface oxidation reaction

$$\theta_{p,ox} = \theta^0 + \frac{1}{\beta}\ln\beta + \frac{1}{\beta}\ln\frac{1}{m} \tag{12}$$

where a plot of peak potential versus the natural logarithm of the inverse sweep rate parameter is linear.

It is possible to derive similar expressions for a reductive surface process and we can show that in such a situation:

$$\begin{aligned} \mathrm{X}_O &= \exp\left[\frac{m}{(1-\beta)}\eta^{-(1-\beta)}\right] \\ \Psi &= m\eta^{-(1-\beta)}\exp\left[\frac{m}{(1-\beta)}\eta^{-(1-\beta)}\right] \end{aligned} \tag{13}$$

and the corresponding peak currents and potentials are given by

$$\begin{aligned} \Psi_p &= -\frac{(1-\beta)}{e} \\ \xi_{p,red} &= \theta_{p,red} - \theta^0 = -\frac{1}{1-\beta}\ln(1-\beta) - \frac{1}{(1-\beta)}\ln\frac{1}{m} \end{aligned} \tag{14}$$

Furthermore we define $\Delta\theta_p = \theta_{p,ox} - \theta_{p,red}$ as the normalized peak potential difference. This parameter can be used to derive useful kinetic information. We can show that

$$\Delta\theta_p = \frac{1}{\beta(1-\beta)}\ln\frac{1}{m} + \ln\left\{\frac{\beta^{1/\beta}}{(1-\beta)^{1/1-\beta}}\right\} \tag{15}$$

Specifically when the transfer coefficient β = 0.5, eqn.15 becomes $\Delta\theta_p = 4\ln m^{-1}$. This expression will be valid with less than 2% error for $m^{-1} > 12$ which occurs for $\Delta E_P > 200$ mV. We can simplify eqn.15 to obtain the following expression from which the standard rate constant k_{ET}^0 can be derived provided that the transfer coefficient β can be evaluated:

$$k_{ET}^0 = \exp\left[F(\beta) - \frac{\beta(1-\beta)F}{RT}\Delta E_p + \ln\left(\frac{F\upsilon}{RT}\right)\right] \tag{16}$$

where

$$F(\beta) = \beta(1-\beta)\ln\left\{\frac{\beta^{1/\beta}}{(1-\beta)^{1/(1-\beta)}}\right\} = \ln\left\{\frac{\beta^{1-\beta}}{(1-\beta)^{\beta}}\right\} \tag{17}$$

Furthermore from eqn.12 and eqn.14 we note that the normalized peak potential ξ_p will vary in a linear manner with the natural logarithm of the inverse scan rate parameter m^{-1}. Now if the linear

portion of the $\xi_{p,ox}$ versus m^{-1} curve is extrapolated to the point where $\xi_{p,ox} = \theta_{p,ox} - \theta^0 = 0$, then at this specific value of the parameter m which we designate as m_{ox}* we note that $\ln\beta + \ln\frac{1}{m_{ox}*} = 0$ or $m_{ox}* = \beta$. This translates to $k_{ET}^0 = \frac{\beta F}{RT}\nu_{ox}*$. Similarly we can show that $k_{ET}^0 = \frac{(1-\beta)F}{RT}\nu_{red}*$. Now we can readily evaluate an expression for the transfer coefficient β by noting that

$$\beta = \frac{1}{1 + \frac{\nu_{ox}^*}{\nu_{red}^*}} \tag{18}$$

We conclude therefore that from eqn.18 and eqn.16 the fundamental kinetic parameters for an irreversible surface process may be determined via measurement of peak potential and peak potential difference as a function of sweep rate.

Transforming eqn.15 we obtain [19] for a single electron transfer reaction:

$$\Delta E_p = \frac{RT}{(1-\beta)\beta F}[\beta\ln(1-\beta) + (1-\beta)\ln\beta - \ln\frac{RT}{F} - \ln k_{ET}{}^0] + \frac{RT}{(1-\beta)\beta F}\ln\upsilon. \tag{19}$$

Peak separations were plotted against lnν for high scan rates (at which the redox process exhibits quasi-reversible/totally irreversible behaviour). Figure 10 shows such a plot for a SWCNT/GOx/Nafion-modified glassy carbon electrode. The slope of this graph was found to be 121 mV, with a y-intercept of 54 mV. Hence from eqn.22 we note that for a n electron transfer reaction $\frac{RT}{(1-\beta)\beta n_\beta F} = 0.121$, where n_β denotes the number of electrons transferred in the rate determining step. This expression results in a quadratic equation in β, which is solved to give values of 0.12 and 0.88 for the transfer coefficient. Adopting β = 0.12 and the intercept value of 0.054 in eqn.22 we get $\frac{RT}{0.88\times0.12\times n_\beta F}\left[0.12\times\ln 0.88 + 0.88\times\ln 0.12 - \ln\frac{RT}{n_\beta F} - \ln k^0\right] = 0.054$, which yields a value of 7.61 s^{-1} for the rate constant for the FAD/$FADH_2$ transformation when suitable values of temperature T and n_β (the latter usually set as unity) are used. It should be pointed out that, because the sum of the transfer coefficients for the oxidation and reduction reactions is unity, the same numerical value for the rate constant is found if the 'other' value obtained for the transfer coefficient is utilized in the calculation. This process was carried out using data obtained for four independently-prepared electrodes and the results are presented in Table 3.

Based on these four values we report a value of 6.1 ± 1.1 s^{-1} for the rate constant. This value is greater than those reported in several other studies of the direct electron transfer of glucose oxidase. On the basis of the Laviron model, it is clear then that the nanotubes used in this work allow for efficient electron transfer. The relative standard deviation of our rate constants is large and, as can be noted in figure 10, the plots themselves may exhibit some deviation from strict linearity (average correlation coefficient around 0.98).

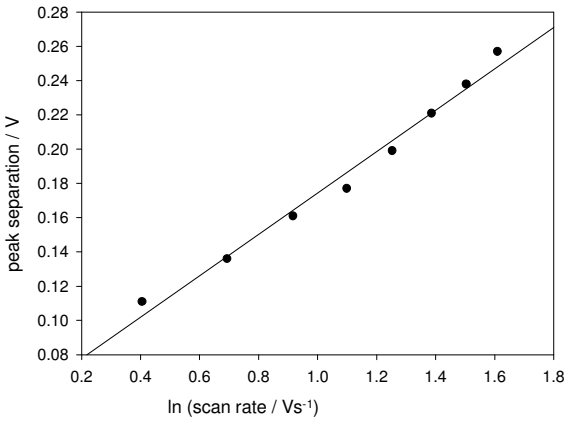

Figure 10. Plot of peak separation against natural logarithm of scan rate for a GC/SWCNT/GOx/Nafion electrode. The electrolyte was a 50 mM phosphate buffer solution (pH 7.0).

Table 3. Summary of rate constants obtained from plots of peak separation against natural logarithm of scan rate for four independently-prepared GC/SWCNT/GOx/Nafion electrodes.

Electrode	Intercept / V	Slope / V	Correlation coefficient	k^0 / s^{-1}
1	0.081	0.160	0.98	5.18
2	0.054	0.121	0.98	7.61
3	0.072	0.146	0.97	5.91
4	0.068	0.150	0.98	5.64

These results may be compared with data previously reported in the literature [27,31]. In this work the apparent heterogeneous electron transfer rate constants for redox proteins and enzymes such as hemoglobin (Hb), horseradish peroxidase (HRP) and Glucose Oxidase (GOx) were determined using linear potential sweep voltammetry at SWCNT modified glassy carbon electrodes to be in the range 1-2 s^{-1}. In contrast Dong and co-workers [32] have examined the kinetics of the microperoxidase 11 redox transformation at glassy carbon electrodes modified with MWCNT meshes. For a microperoxidase loading of 0.84 nmol cm^{-2} a standard rate constant of 38 s^{-1} was determined. It is clear that the standard heterogeneous rate constant for adsorbed redox proteins and enzymes can vary somewhat and lie between 1-40 s^{-1} when cyclic voltammetry measurements are made in phosphate buffer solution on CNT meshes. To date nearly all attempts to quantify the redox kinetics of adsorbed enzymes and redox proteins using electrochemical techniques have involved use of the Laviron theory [19] which is cast in a form which describes specifically the current response to an applied linear potential sweep. This model neglects the effect of kinetic dispersion which may be very significant for

high surface area systems like SWCNT meshes adsorbed on support electrode surfaces. In the next section we suggest that the technique of potential step chronoamperometry provides a very convenient method to both identify, and monitor the extent of, kinetic dispersion in a surface adsorbed redox system and we examine the response of the GOx immobilized on SWCNT /Nafion modified glassy carbon electrodes.

We contend therefore that the Laviron analysis of the reactivity of surface immobilized redox groups is too simple and needs to be subjected to a more realistic level of analysis. The AFM image presented in figure 1 clearly shows that the nanotube film is completely disordered. Also, variations in nanotube conductivity and the fact that the enzyme is almost certainly not oriented in a uniform manner throughout the nanotube matrix must surely serve to broaden the spread in kinetic site activity. Hence we conclude that kinetic dispersion must be considered and factored into any realistic kinetic analysis.

3.3.2. Potential Step Chronoamperometry: surface redox process.

Cyclic voltammetry does not always provide the optimum route to kinetic parameters. It can be difficult to distinguish between Ohmic drop and kinetic effects when investigating the variation of the voltammetric response with sweep rate. Potential step techniques may be used with profit to calculate electron transfer rate constants for redox systems immobilised on electrodes.

The carbon nanotube mesh modified electrode has a rather large surface area and so one might expect that the differential capacitance of the modified electrode/solution interface would be significant. Hence the charging current contribution to the observed current flow either during a potential sweep experiment or a potential step experiment could well be significant. The extraction of kinetic information would consequently require a clear decoupling of the Faradaic and double layer charging contributions [34]. Consequently we evaluated the interfacial capacitance of a SWCNT modified glassy carbon electrode in pH 7 phosphate buffer solution using cyclic voltammetry and potential step chronoamperometry. It is readily shown that the charging current contribution arising from a linear potential sweep is given by

$$i_C = C_{DL}\upsilon + \left(\frac{E_i}{R_S} - C_{DL}\upsilon\right)\exp\left[-\frac{t}{R_S C_{DL}}\right] \tag{20}$$

where C_{DL} and R_S denotes the double layer capacitance and solution resistance respectively and ν denotes the sweep rate. The corresponding expression for the charging current response to an applied potential step of amplitude ΔE is:

$$i_C = \frac{\Delta E}{R_S}\exp\left[-\frac{t}{R_S C_{DL}}\right] \tag{21}$$

Two points are important to note. The first (from eqn.20) is that the charging current observed during a potential sweep experiment consists of both a steady state and a transient contribution. The current rises from zero as the scan starts and attains a steady value given by $C_{DL}\upsilon$. Hence we predict that a plot of charging current i_C versus sweep rate ν should be linear if a current reading is chosen at a suitable time during the potential sweep experiment where the transient contribution has decayed. The second

point to note concerns the potential step experiment expression outlined in eqn.21. Here a plot of $\ln i_C$ versus time t is linear with a slope given by $-1/R_S C_{DL}$ and an intercept given by $\Delta E/R_S$.

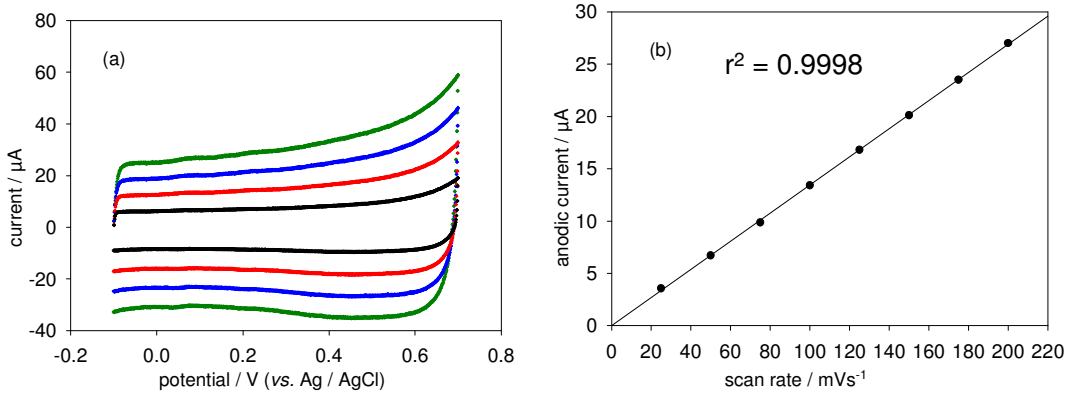

Figure 11. (a) Cyclic voltammograms of a carbon nanotube-modified glassy carbon electrode in a pH 7.0 phosphate buffer. Scan rates were (from inner to outer) 50, 100, 150 and 200 mVs^{-1}. **(b)** The resulting plot of anodic peak current at +0.1 V against scan rate.

The results obtained for a series of potential sweep measurements conducted on a SWCNT modified glassy carbon modified electrode in phosphate buffer solution pH 7 over a range of sweep rates (25-200 mV/s) are presented in figure 11. In the potential window of -0.1 to +0.7 V (*vs.* Ag / AgCl), the voltammograms were found to be featureless, showing no discernible redox peaks. Slight increases in anodic current were observed at high potentials and these were attributed to the partial oxidation of the solvent. In order to evaluate the capacitance, values for the anodic current at a potential of +0.1 V were plotted against scan rate, as shown in Figure11(b). This low potential was selected so contributions from solvent oxidation could be ruled out. It was also a value where the transient contribution to the charging current could be readily neglected. Good linearity between current and sweep rate is observed and the slope of the curve is 0.134 mF. Combining this with a calculated modified electrode surface area of (9.76 ± 0.98) × 10^{-2} cm^2 obtained from a separate cyclic voltammetric analysis of ferricyanide reduction at the SWCNT modified glassy carbon electrode (data not shown), we obtained a surface specific capacitance of roughly 1.4 $mFcm^{-2}$, which is similar to values found elsewhere for various nanotubes cast from DMF suspensions [35]. An estimate of the total uncompensated solution resistance R_S can be obtained from complex impedance spectroscopy. The result of the latter experiment is presented in figure 12. Here the impedance spectrum of the nanotube mesh modified glassy carbon electrode recorded at open circuit in phosphate buffer solution is presented. The AC signal applied to the electrode was 5 mV in amplitude. Data were collected at the open circuit potential (+0.17 V *vs.* Ag / AgCl) in the frequency range 10^{-2} to 10^5 Hz. The resulting Nyquist plot was dominated by a large, well-defined, linear Warburg diffusive feature, indicating that the transfer of charge across the buffer / nanotube interface was facile. The high frequency real axis intercept of the Nyquist plot for the SWCNT modified electrode is close to 125 Ω which can be equated to the solution resistance R_S. Hence the time constant for the SWCNT modified glassy carbon electrode is $\tau = R_S C_{DL} \cong 0.017\, s \approx 17\, ms$.

Hence we note that the lower limit of the experimental timescale used to extract kinetic information on the redox transformation of the flavin moiety within the immobilized enzyme will be dependent on the magnitude of the charging time constant τ . The latter value extends into the millisecond time regime for the highly dispersed SWCNT mesh electrodes examined in this work. This is unlike the tens of microsecond timescale usually observed for simple planar electrodes in contact with dilute aqueous solution. Hence it may well be difficult to totally deconvolute the charging component of the current from the experimentally observed total current if the kinetics of the surface redox reaction are very rapid (as they may well be).

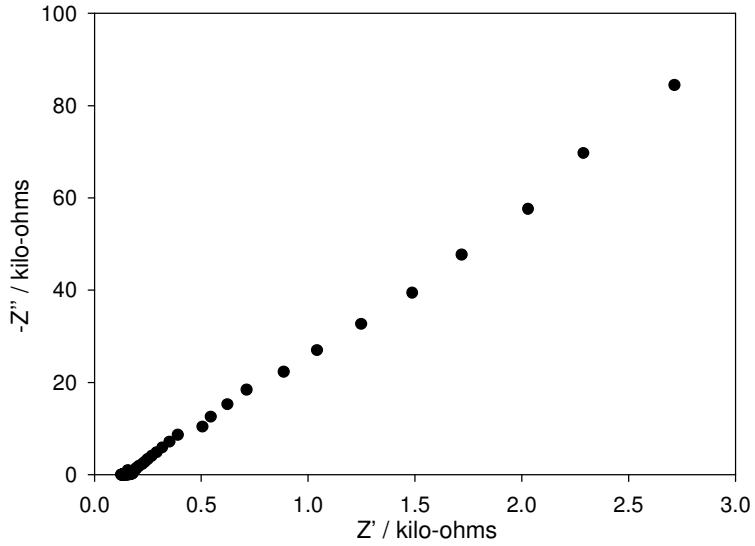

Figure 12. Complex impedance Nyquist plots for a nanotube-modified glassy carbon electrodes at +0.17 V (*vs.* Ag / AgCl) in a pH 7 phosphate buffer solution (50 mM).

As previously noted potential step chronoamperometry can also provide a direct measurement of the double layer charging time constant. The result of a typical chronoamperometry experiment is presented in figure 13. Here the current response to a potential step from 0 to 50 mV (vs Ag/AgCl) is presented along with a plot of $\ln i$ versus time. The excellent linearity exhibited by the latter indicates that the chronoamperometric profile is well described by eqn.21.

The current intercept at zero time is $\ln i_0 = \ln(\Delta E / R_S) = -8.14$ and noting that $\Delta E = 0.05\,V$, then we estimate $R_S \cong 171\,\Omega$. Furthermore the slope of the linear semilogarithmic plot was $1/R_S C_{DL} = 43.9\,s^{-1}$ and correspondingly the double layer charging time constant is estimated as $\tau = 23\,ms$ and the double layer charging current is 0.134 mF. The latter is in good agreement with that estimated from a combination of potential sweep voltammetry and complex impedance spectroscopy. The analysis was repeated for a number of potential step amplitudes and the results are presented in table 4 below. Similar experiments were performed using unmodified glassy carbon electrodes and for a pulse width of 50 mV values of $R_S = 650\,\Omega, C_{DL} = 0.017\,mF, \tau = 11\,ms$ were obtained.

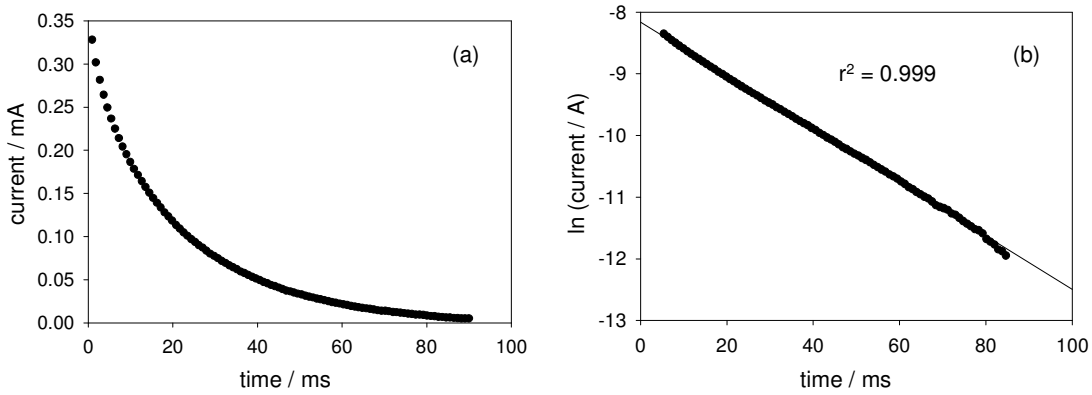

Figure 13. Potential step chronoamperometry at a carbon nanotube-modified glassy carbon electrode in a pH 7 phosphate buffer solution (50 mM). Potential stepped from an initial value of 0 V to 50 mV (vs Ag/AgCl). (a) Current time response profile. (b) semilogarithmic analysis of chronoamperometric data.

Table 4. Double layer charging capacitance and solution resistance data obtained via potential step chronoamperometry experiments with various pulse widths.

ΔE / mV	**R_S / Ω**	**C_{DL}/mF**	**τ / ms**
50	171	0.134	23
100	186	0.134	25
150	191	0.141	27
200	196	0.143	28

It is interesting to note that $C_{DL}(GC/NT)/C_{DL}(GC) \cong 7.9$ which provides a good estimate of the roughness factor of the mesh modified electrode compared with the corresponding unmodified glassy carbon electrode surface.

Bearing the results obtained for interfacial charging in mind the potential step chronoamperometry technique was applied to a GC/SWCNT/GOx/Nafion modified electrode. In this experiment the potential was poised at -0.6 V (*vs.* Ag / AgCl) for five minutes in order to ensure that only the reduced form of the prosthetic group was present. The potential was then stepped to -0.2 V and the current response was monitored for a pulse width of 0.4 seconds, which was found to be sufficient to allow the signal to decay to a steady-state value. The raw data are presented in Figure 13(a). The estimated charging time constant (*vide infra*) is small compared with the pulse width of 0.4 s used in our experiments (figure 14(a)) and it can be concluded that the measured current data obtained are representative of the faradaic behaviour of glucose oxidase on the electrode surface. The raw data was then recast in semi-logarithmic form for subsequent data analysis (figure 14(b)).

The analysis of the current versus time response to a potential step of arbitrary magnitude has been recently described by Lyons [33]. We review this material for convenience here. We initially

consider the transient current response obtained to a large amplitude potential step perturbation applied to a surface immobilized redox couple A/B. We let Γ_j (j = A,B) represent the surface coverage (units: mol cm^{-2}) of component j of the redox couple, and define the total surface coverage as $\Gamma_\Sigma = \Gamma_A + \Gamma_B$. We initially assume that the surface redox reaction is irreversible with a rate equation given by:

$$-\frac{d\Gamma_A}{dt} = \frac{d\Gamma_B}{dt} = k_{ET}\Gamma_A \tag{22}$$

where the heterogeneous electrochemical rate constant (units: s^{-1}) is of the Butler-Volmer type and is given by

$$k_{ET} = k_{ET}{}^0 \exp[\beta\xi] \tag{23}$$

where k^0 denotes the standard rate constant, β is the symmetry factor and ξ denotes a normalized potential given by $\xi = \frac{F}{RT}\left(E - E^0_{A/B}\right)$. The current response to the applied potential step is given by

$$i(t) = nFAf_\Sigma(t) = nFAk_{ET}\Gamma_A(t) \tag{24}$$

where f_Σ denotes the net flux (units: mol cm^{-2} s^{-1}), n denotes the number of electrons transferred in the surface redox process, A denotes the geometric area of the electrode and F is the Faraday constant.

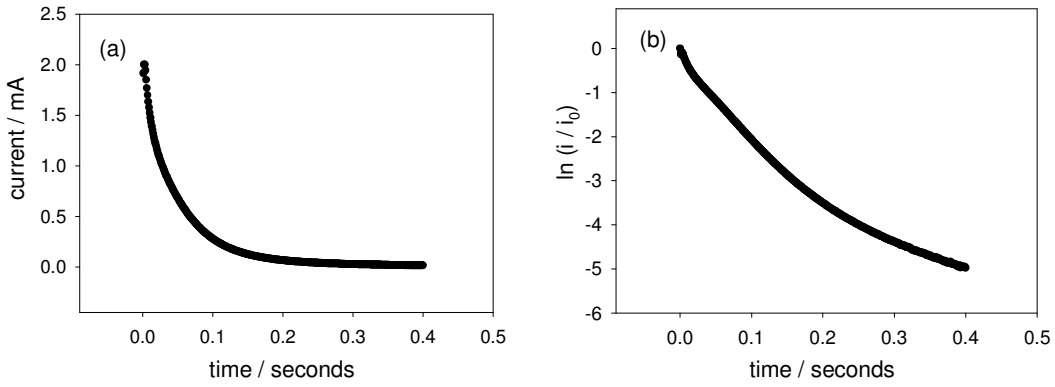

Figure 14. (a) Chronoamperometric response to a potential step experiment across the FAD oxidation potential for a GC/SWCNT/GOx/Nafion electrode. The electrolyte used was a 50 mM PBS (pH 7.0). (b) The resulting plot for the determination of the rate constant, based on the assumption of first-order kinetics.

The variation of surface coverage with time is obtained via integration of eqn.22 subject to the initial condition that at $t = 0 \quad \Gamma_A = \Gamma_\Sigma$. Hence integration of eqn.22 immediately yields

$$\Gamma_A(t) = \Gamma_\Sigma \exp[-k_{ET}t] \tag{25}$$

and the surface redox transition obeys first order kinetics. Hence the current response is expected to follow a simple exponential decay and is given by

$$i(t) = k_{ET}Q\exp[-k_{ET}t] \tag{26}$$

where the charge Q is related to the surface coverage of electroactive groups via the expression $Q = nFA\Gamma_{\Sigma}$. This expression has been used by Finklea [36], Chidsey [37] , Miller and co-workers [38] and by Forster and Faulkner [39] to examine the dynamics of self assembled monolayer systems. Hence we conclude that the variation of current with time for a simple surface redox transformation is described by simple first-order kinetics. This means that, ideally, a plot of natural logarithm of the current against time should be linear, with a slope giving directly the heterogeneous electrochemical rate constant k_{ET}. This result is quite unlike the situation found with a redox couple free to diffuse in solution to an electrode where the Faradaic component of the current varies as the inverse square root of the time. For surface redox reactions both the charging and Faradaic contributions to the observed current vary in an exponential manner with time.

We can readily extend the analysis to consider a quasi-reversible surface reaction. In this case the rate equation for the surface redox reaction is given by

$$-\frac{d\Gamma_A}{dt} = k_{ET}\Gamma_A - k'_{ET}\Gamma_B \tag{27}$$

where the heterogeneous rate constant for the reverse step is given by $k'_{ET} = k_{ET}{}^{0}\exp\left[-(1-\beta)\xi\right]$. We can integrate eqn.27 using the initial condition $t = 0 \quad \Gamma_A = \Gamma_{\Sigma} \quad \Gamma_B = 0$ to obtain

$$\Gamma_A(t) = \Gamma_{\Sigma}\left\{\frac{1+(k_{ET}/k'_{ET})\exp\left[-k_{\Sigma}t\right]}{1+(k_{ET}/k'_{ET})}\right\} \tag{28}$$

where we note that $k_{\Sigma} = k_{ET} + k'_{ET}$. At any time t we also note that $\Gamma_A(t) + \Gamma_B(t) = \Gamma_{\Sigma}$ and so we also obtain that

$$\Gamma_B(t) = \Gamma_{\Sigma}\left\{\frac{(k_{ET}/k'_{ET})\left(1-\exp\left[-k_{\Sigma}t\right]\right)}{1+(k_{ET}/k'_{ET})}\right\} \tag{29}$$

The net current response is therefore given by

$$i(t) = nFA\left\{k_{ET}\Gamma_A(t) + k'_{ET}\Gamma_B(t)\right\} \tag{30}$$

From eqn.28, eqn.29 and eqn.30 we immediately obtain

$$i(t) = nFAk_{\Sigma}\Gamma_{\Sigma}\exp\left[-k_{\Sigma}t\right] = i_0\exp\left[-k_{\Sigma}t\right] \tag{31}$$

Again a simple exponential decay in current with time is predicted. A plot of $\ln i$ versus t is linear with intercept given by $nFAk_{\Sigma}\Gamma_{\Sigma}$ and a slope given by $-k_{\Sigma}$. Hence the surface redox kinetics can be completely resolved using the potential step technique.

As previously noted figure 14(a) shows a plot of the logarithm of the normalised current against time obtained for the oxidation of $FADH_2$ and the reduction of FAD at a SWCNT/GOx/Nafion-modified glassy electrode. It can be seen that the chronoamperometric transients displayed in Figure 14(b) are not linear. Consequently the prediction of a simple first order kinetic situation is not maintained experimentally, and the theoretical analysis must be adjusted accordingly. It is also clear that the deviation of the semilogarithmic plot from simple linear first order kinetic behaviour presents in a very direct way the fact that the surface redox kinetics are more complex than expected . This is a

compelling reason why the technique of potential step chronoamperometry is to be preferred over that of cyclic voltammetry.

This discrepancy can probably be attributed to the energetic non- equivalence of the GOx molecules on the nanotubes. It is safe to assume that the orientation of the protein structure with respect to the nanotube platform is not uniform. This means that the FAD sites in each molecule are various distances from the nanotubes, so a variation in the magnitude of the rate constant quantifying the ET kinetics between the flavin active site and the nanotube surface is observed. There exists an undefined spatial relationship between the protein and the SWCNTs. Furthermore, some sites on the nanotubes are more active than others due to the presence or absence of oxygenated defects. Also, it has been established that SWCNTs show a range of conductivity [1]. These factors all serve to increase the spread of observed rate constants. We should note however that the shape of chronoamperometric response profiles and linear potential sweep voltammograms can be affected not only by kinetic dispersion effects, but also by the existence of a distribution in electric potential across the adsorbed molecule surface layer. The manner in which an interfacial potential distribution effects the voltammetric response of a surface immobilized redox active moiety has been reported by Smith and White [21], Murray and co-workers [40] and Honeychurch [41] and for potential step chronoamperometry by Creager and Weber [42]. We do not address this possibility in the present paper but focus attention solely on kinetic dispersion effects.

3.3.3. Potential Step Chronoamperometry: surface redox process with a Gaussian kinetic dispersion.

Typically when heterogeneous systems such as hydrated oxide thin films, fluorescence decay in membranes, semiconductor nanoparticle dispersions are subjected to a kinetic analysis, curved semilogarithmic plots are often observed (as presented in figure 19) when the data is tested for first order kinetics. Albery and co-workers [13] have proposed that it is possible to present an alternative model for kinetics in these dispersed systems. In this approach one assumes a Gaussian distribution in the free energy of activation for the kinetic process and consequently in the logarithm of the rate constant about some mean value. In short a log-normal distribution is assumed [43]. Hence one single adjustable parameter is only introduced- the width γ of the distribution. When $\gamma = 0$ there is no dispersion and the system behaves in a classical homogeneous fashion and first order kinetics are observed.

We assume that the free energy of activation for the enzyme redox process is given by the following expression

$$\Delta G^* = \langle \Delta G^* \rangle - RT\gamma\chi \tag{30}$$

where $\langle \Delta G^* \rangle$ denotes the mean free energy of activation and γ denotes the spread parameter. The quantity χ denotes the co-ordinate characterizing the Gaussian Distribution. Note that when $\gamma = 0$ $\Delta G^* = \langle \Delta G^* \rangle$ and there is no dispersive spread. The kinetics are simple first order. We define $\langle k_{ET} \rangle$ to be the heterogeneous electron transfer rate constant for the most probable state and write that the dispersion in first order rate constants is

$$k_{ET} = \langle k_{ET} \rangle \exp[\gamma\chi] \tag{31}$$

We also define a normalized time τ related to the mean rate constant $\langle k_{ET} \rangle$ via $\tau = \langle k_{ET} \rangle t$. Now the first order rate equation for surface adsorbed enzyme is given by

$$-\frac{d\Gamma}{dt} = k_{ET}\Gamma = \langle k_{ET} \rangle \exp[\gamma\chi]\Gamma \tag{32}$$

Integrating we obtain

$$\int_{\Gamma_{x,0}}^{\Gamma_{x,t}} \frac{d\Gamma}{\Gamma} = -\langle k_{ET} \rangle \exp[\gamma\chi] \int_0^t dt \tag{33}$$

and so simplifying we obtain

$$\frac{\Gamma_\chi(\tau)}{\Gamma_{\chi,0}} = \exp\left[-\tau \exp[\gamma\chi]\right] \tag{34}$$

We now integrate across the Gaussian distribution and note that the decay of the surface concentration of species Γ from their initial value Γ_0 is given by

$$\frac{\Gamma}{\Gamma_0} = \frac{\int_{-\infty}^{\infty} \exp\left[-\chi^2\right].\exp\left[-\tau \exp[\gamma\chi]\right] d\chi}{\int_{-\infty}^{\infty} \exp\left[-\chi^2\right] d\chi} = \frac{1}{\sqrt{\pi}} \int_{-\infty}^{\infty} \exp\left[-\chi^2\right].\exp\left[-\tau \exp[\gamma\chi]\right] d\chi \tag{35}$$

where we note that the Gaussian integral takes the following form

$$\int_{-\infty}^{\infty} \exp\left[-\chi^2\right] d\chi = \sqrt{\pi} \tag{36}$$

It is satisfactory to note that when γ = 0 corresponding to the absence of kinetic dispersion, eqn. 35 reduces to

$$\frac{\Gamma}{\Gamma_0} = \exp[-\tau] \tag{37}$$

corresponding to simple first order exponential decay.

Now the net current i is given by:

$$\begin{aligned} i &= nFAf_\Sigma = nFAk_{ET}\Gamma = nFA\langle k_{ET} \rangle \Gamma \\ &= nFA\langle k_{ET} \rangle \Gamma_0 \pi^{-1/2} \int_{-\infty}^{\infty} \exp[\gamma\chi] \exp\left[-\chi^2\right] \exp\left[-\tau \exp[\gamma\chi]\right] d\chi \end{aligned} \tag{38}$$

We have previously shown [44] that the integral in eqn.38 may be expressed in the following form:

$$I(\gamma, \chi, \tau) = \int_{-\infty}^{\infty} \exp[\gamma\chi] \exp\left[-\chi^2\right] \exp\left[-\tau \exp[\gamma\chi]\right] d\chi = \int_0^1 G(\lambda)\, d\lambda \tag{39}$$

where

$$G(\lambda) = \lambda^{-1} \exp\left[-(\ln \lambda)^2\right]\left\{\lambda^{\gamma} \exp\left[-\lambda^{\gamma}\tau\right] + \lambda^{-\gamma} \exp\left[-\lambda^{-\gamma}\tau\right]\right\} \tag{40}$$

and we have adopted the following transformations

$$\begin{aligned} &\chi < 0 \quad \chi = \ln \lambda \quad d\chi = \lambda^{-1} d\lambda \\ &\chi > 0 \quad \chi = -\ln \lambda \quad d\chi = -\lambda^{-1} d\lambda \end{aligned} \tag{41}$$

and

$$\begin{aligned} &\chi = \pm\infty \quad \lambda = 0 \\ &\chi = 0 \quad \lambda = 1 \end{aligned} \tag{42}$$

Hence the current transient may be computed from eqn.38 using eqn.39 and eqn.40. Similarly, the integral outlined in eqn.35 may be integrated in a similar manner

$$\begin{aligned} \frac{\Gamma}{\Gamma_0} &= \frac{1}{\sqrt{\pi}} \int_{-\infty}^{\infty} \exp\left[-\chi^2\right].\exp\left[-\tau \exp[\chi]\right] d\chi \\ &= \frac{1}{\sqrt{\pi}} \int_0^1 F(\lambda)\, d\lambda \end{aligned} \tag{43}$$

where

$$F(\lambda) = \lambda^{-1} \exp\left[-(\ln \lambda)^2\right]\left\{\exp\left[-\lambda^{\gamma}\tau\right] + \exp\left[-\lambda^{-\gamma}\tau\right]\right\} \tag{44}$$

The population of Gaussian distributed redox states computed numerically via the extended Simpsons rule [44] with $\gamma = 2$ is outlined in figure 15.

We note from this 3D surface plot calculated from eqn.43 that as the reaction proceeds (as τ increases) the original symmetrical Gaussian profile becomes skewed to those species with lower rate constants. These slower species predominate in the latter stages of a chronoamperometric experiment giving rise to the type of curvature seen in the double-logarithmic plots presented in figure 17. It should be noted that when analyzing current transients the faster redox sites make a greater contribution to the observed redox current.

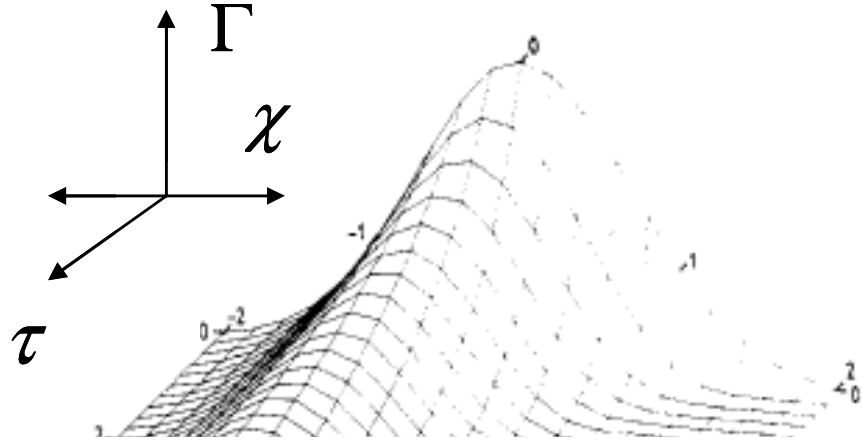

Figure 15. The decay of the Gaussian population calculated using eqn.43 with spread parameter $\gamma = 2$.

The variation of Γ/Γ_0 *vs* τ for various values of the spread parameter g is outlined in figure 16, and typical current transient response curves calculated from eqn.38 are illustrated in figure 17. We note from figure 17 that the current decays more rapidly as the numerical value of the Gaussian spread parameter g increases.

Alternatively, to determine a value of the spread parameter from experimental data one can follow the procedure originally suggested by Albery and co-workers [13]. In this work it was suggested that the ratio of $\tau_{7/8}$ to $\tau_{1/2}$ be measured where $\tau_{1/2}$ defined the half life of the reaction and $\tau_{7/8}$ defines the time when one eight of the original reactant species remains. The following empirical relationship between γ and the latter parameters has been proposed:

$$\gamma = 0.92 \times \left(\frac{\tau_{7/8}}{\tau_{1/2}} - 3 \right)^{1/2} \tag{45}$$

It was also suggested that the mean rate constant could be evaluated from the latter relationship

$$\langle k_{ET} \rangle = \frac{1}{\tau_{1/e}} \tag{46}$$

where $\tau_{1/e}$ is the time when the current has decayed to 1/e (~0.37) of its initial value. In practical terms, this is simply the time when the ratio i / i_0 is approximately 0.63, or ln (i /i_0) is around -0.46.

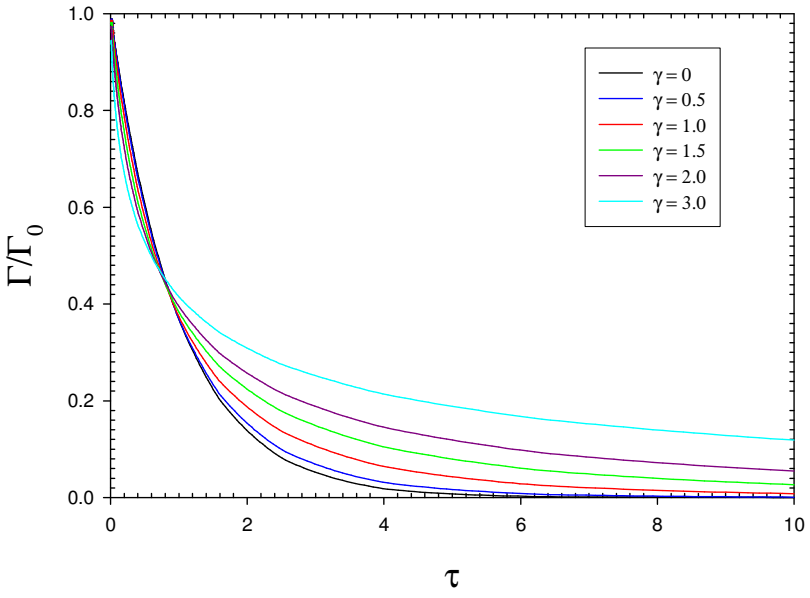

Figure 16. Typical concentration transients calculated from eqn.43 for various values of the spread parameter γ.

In their 1985 paper, Albery and co-workers [13] reported that if the decay of some property λ (where λ is proportional to concentration, *c*) could be experimentally measured with time, experimentally based plots of $\ln(\lambda/\lambda_0)$ against $\ln t$ could be matched against theoretically derived working curves of $\ln(c/c_0)$ *versus* $\ln \tau$ calculated using eqn 43. By adjusting the displacements of the experimental

curve on both axes, matching data to a particular theoretical curve produced a value for the dispersion parameter γ.

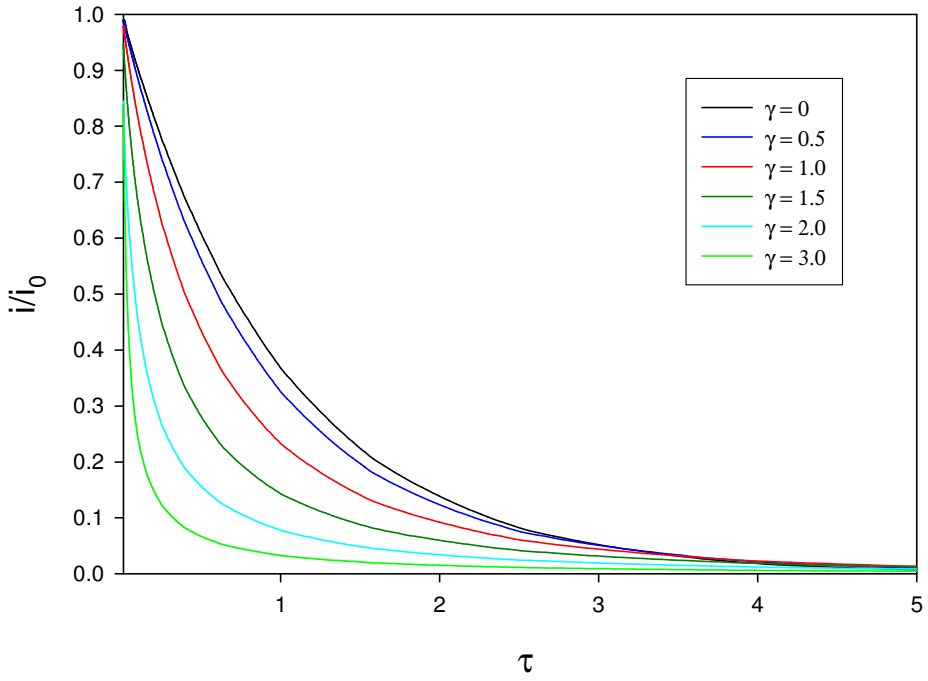

Figure 17. Typical normalized current transients calculated from eqn.38, for various values of the spread parameter γ, illustrating the effect of kinetic dispersion.

The current flowing across an interface is the rate at which charge is being transferred, so if a current-time transient for a potential step such as the one shown in Figure 14(a) is integrated, the result is a *charge*-time transient showing how the quantity of charge transferred, *Q(t)*, *increases* with time. The result of such an operation is presented in Figure 18(a). If Q_{tot} is the total amount of charge transferred after a potential step, we may define W as the fraction of the total charge *remaining* to be transferred at a given time and write:

$$W = \frac{Q_{tot} - Q(t)}{Q_{tot}} = \frac{\Gamma}{\Gamma_0} \qquad (47).$$

Like the normalised surface coverage Γ/Γ_0, this number W decays from unity to zero during the course of an experiment as illustrated in figure 18 (b).

The point is that W, unlike the normalised current, may be considered as representing the normalised surface coverage. They have the same value at all times during a potential step experiment. This means, for example, that if 80 % of the total charge has been transferred at a given time, W has the value 0.2 and it is correct to infer that 80 % of the active sites have reacted at that time. It would not be reasonable to claim this on the basis of the *current* losing 80 % of its initial value. So values for

the dispersion parameter may be obtained by fitting plots of $\ln W$ against $\ln t$ to theoretical plots of $\ln(\Gamma/\Gamma_0)$ against $\ln \tau$ drawn using eqn.43.

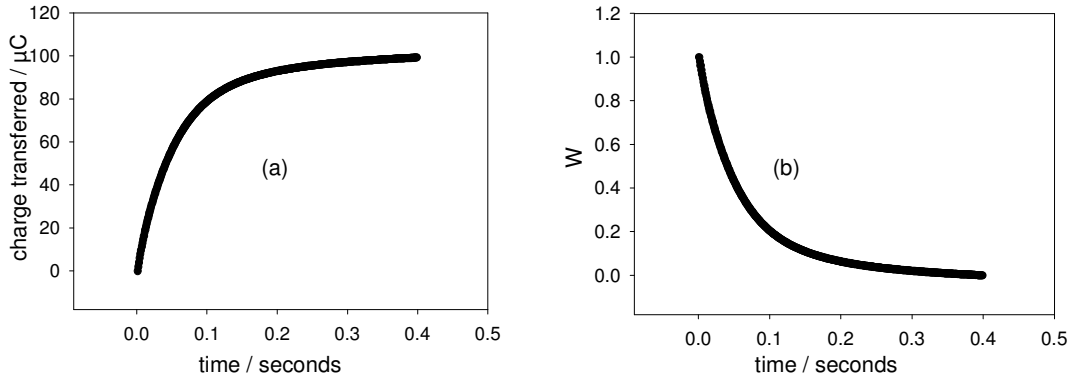

Fig. 18(a) Chronocoulometric response to a potential step experiment across the FAD oxidation potential for a GC/SWCNT/GOx/Nafion electrode, obtained by the integration of the curve shown in Figure 14(a). The electrolyte used was a 50 mM phosphate buffer solution (pH 7.0). (b) The resulting plot showing the decay of *W*, as defined in *Equation 47*.

Rather than fitting data to working curves, values for γ and also, importantly, the *mean rate constant* may be found using the procedure originally suggested by Albery and co-workers [13]. These two values may be obtained using the simple expressions presented in eqn.45 and eqn.46 and extracting the relevant parameters from a semi-logarithmic plot such as that shown in Figure 19(a).

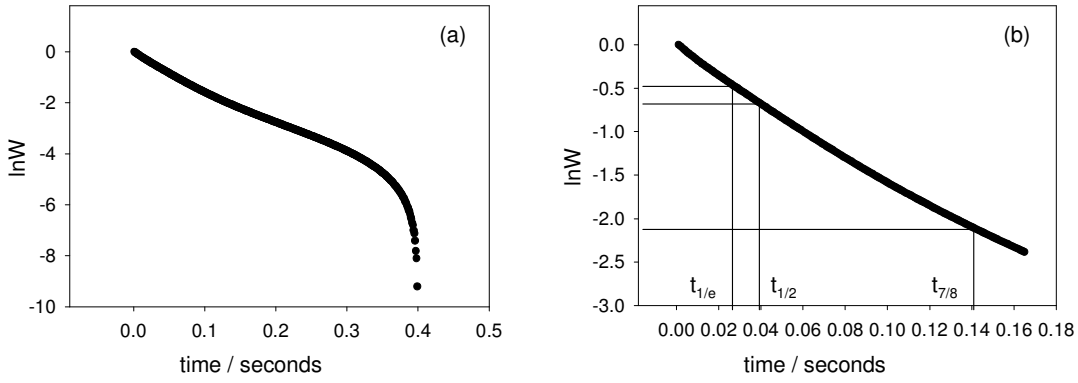

Figure 19(a) Semi-logarithmic plot showing the decay of *W*, based on data from the previous figure. (b) Close-up of the short-time region, showing how the relevant times were estimated for the calculation of the mean rate constant and the spread parameter.

Now $\tau_{7/8}$ is the time at which W has lost 7/8 (i.e. 0.875) of its initial value. This is when W = 0.125 and $\ln W$ = - 2.08 (see figure 19 (b)). Furthermore $\tau_{1/e}$ is the time at which W has lost 1/e or ca 37% of

its initial value. This occurs when W = 0.63 or when $\ln W$ = - 0.46 (figure 19(b)) and so $\tau_{1/e} = 0.028$ s. The time at which W is half its initial value is $\tau_{1/2}$, which corresponds to $\ln W$ = -0.69. Detailed analysis of the experimental data presented in figure 19(b) and using eqn.45, afforded values of 0.14 s and 0.04 s for $\tau_{7/8}$ and $\tau_{1/2}$ respectively, yielded a value of γ = 0.65 for the spread parameter. Direct application of eqn.46 with $\tau_{1/e} = 0.028\,s$, afforded $\bar{k} = 35.71\,s^{-1}$. This corresponds to the first order rate constant for Flavin oxidation. When the same experiment and analysis were carried out for a cathodic step, poising the potential at -0.2 V (*vs.* Ag / AgCl) and stepping to -0.6 V, values of 33 s^{-1} and 0.58 were obtained for the flavin reduction rate constant and spread parameter, respectively. These values are somewhat larger than those obtained via the Laviron analysis. However it should be noted that significant double layer charging effects may well be still operative in the time scales where the characteristic time parameters were measured. These values for the rate constant are in good accord with values recorded for other bound enzyme systems as reported in the literature.

4. CONCLUSIONS

In this paper we have reported in detail on the redox behaviour of SWCNTs randomly dispersed on gold and glassy carbon electrode surfaces. We have used a simple technique to adsorb glucose oxidase onto SWCNT-modified gold and glassy carbon electrodes and shown that well defined voltammetric responses can be obtained at these enzyme modified nanotube meshes and the kinetics of the FAD/$FADH_2$ redox transformation may be directly quantified. We have also demonstrated that adsorbed enzymes exhibit significant kinetic dispersion, and that the dispersion is best subjected to analysis via potential step chronoamperometry. This conclusion is in contrast to current practice where linear potential sweep voltammetry is often the technique adopted for the quantitative analysis of kinetic data of surface immobilized redox species. We have also noted that double layer charging effects may well be an important component of the current observed during a potential step experiment. This is because of the highly dispersed nature of the nanotube mesh on the support electrode surface. In our quantitative analysis we have utilised a sophisticated analysis developed some years ago by Albery [13], which assumes that curved, semi-logarithmic kinetic plots can be fitted using a Gaussian kinetic model. The extension of the Gaussian kinetic model to linear potential sweep voltammetry is currently underway and a modification of the Laviron theory to account for kinetic dispersion effects will be reported in a subsequent paper. In part 2 of the present series of papers the catalytic activity of the SWCNT/GOx/ Nafion modified electrode system with respect to glucose oxidation will be addressed.

ACKNOWLEDGEMENT

The authors are grateful for the financial support of Enterprise Ireland, Grant number SC/2003/0049, IRCSET Grant Number SC/2002/0169 and the HEA-PRTLI Program. We also acknowledge the very helpful comments provided by Professor Robert Forster, Dublin City University regarding the influence of double layer charging effects on chronoamperometric transients.

References

1. S. Iijima , *Nature* 354(1991) 56.
2. (a) J.J. Goodring, *Electrochim. Acta* 50 (2005) 3049 (b) J.Wang, *Electroanalysis*, 17 (2005) 7.
3. E. Katz, I. Willner, *ChemPhysChem*., 5 (2004) 1084.
4. A.M. Kuznetsov, J. Ulstrup, *Electron transfer in chemistry and biology*, Wiley, New York (1998).
5. K. Habermuller, M. Mosbach, W. Schuhmann, *Fresenius J. Anal. Chem.,* 366 (2000) 560.
6. W. Schuhmann, *Rev. Mol. Biotechnol.,* 82 (2002) 425.
7. A. Guiseppi-Elie, C. Lei, R.H. Baughman, *Nanotechnology,* 13 (2002) 559.
8. J.X. Wang, M. Musameh, Y. Lin, *J. Am. Chem. Soc.,* 125 (2003) 2408.
9. J. Wang, M. Musameh, *Anal. Chem.,* 75 (2003) 2075.
10. G. Wang, J.J. Xu, H.Y. Chen, *Electrochem. Commun.*, 4 (2002) 506.
11. K. Yamamoto, G. Shi, T.Zhou, F. Xu, J. Xu, T. Kato, J.J. Jin, L. Jin, *Analyst* 128 (2003) 249.
12. (a) J.J. Goodring, R. Wibowo, J. Liu, W. Yang, D. Losic, S. Orbons, F.J. Mearns, J.G. Shapter, D.B. Hibbert, *J. Am. Chem. Soc*. 125 (2003) 9006. (b) J. Liu, A. Chou, W. Rahmat, M.N. Paddon-Row, J.J. Goodring, *Electroanalysis* 17 (2005) 38.
13. W.J. Albery, P.N. Bartlett, C.P. Wilde, J.R. Darwent, *J. Am. Chem. Soc.* 107 (1985) 1854.
14. R.S. Nicholson, *Anal. Chem.* 37 (1965) 1351.
15. J.M. Nugent, K.S.V. Santhanam, A. Rubio, P.M. Ajayan, *Nano Lett.*1 (2001) 87.
16. C. Cai, J. Chen, *Anal. Biochem.* 332 (2004) 75.
17. P. Diao, Z. Liu, *J. Phys. Chem. B.* 109 (2005) 20906.
18. A.J. Bard, L.R. Faulkner, *Electrochemical Methods*, Wiley, New York,. Chapter 10, pp.368-416 (2001).
19. E. Laviron, *J. Electroanal. Chem.* 101 (1979) 19.
20. M.J. O'Connell, P. Boul, L.M. Ericson, C. Huffman, Y.Wang, E. Haroz, C. Kuper, J. Tour, K.D. Ausman, R.E. Smalley, *Chem. Phys. Lett.,* 342 (2001) 265.
21. (a) C.P. Smith, H.S. White, *Anal. Chem.*, 64 (1992) 2398. (b) M. Ohtani, S. Kuwabata, H. Yoneyama, *Anal. Chem*. 69 (1997) 1045.
22. (a) A.P. Brown, F.C. Anson, *Anal. Chem*., 49 (1977) 1589. (b) M.J. Honeychurch, G.A. Rechnitz, *Electroanalysis.* 10 (1998) 285. (c) M.J. Honeychurch, G.A. Rechnitz, *Electroanalysis*. 10 (1998) 453.
23 I.M. Shiryava, J.P. Collman, R. Boulatov, C.J. Sunderland, *Anal. Chem.,* 75 (2003) 494.
24. J. Li, A. Cassell, L. Delzeit, J. Han, M. Meyyappan, *J. Phys. Chem. B* 106 (2002) 9299.
25. L. Roullier, E. Laviron, *J. Electroanal. Chem.* 157 (1983) 193.
26. A. Szucs, G.D. Hitchens, J.O'M. Bockris, *J. Electrochem. Soc*., 136 (1989) 3748.
27. W. Liang, Y. Zhuobin, *Sensors,* 3 (2003) 544.
28. G. Wang, N.M. Thai, S-T Yau, *Electrochem. Commun.* 8 (2006) 987.
29. J.J. Gooding, M. Situmorang, P. Erokhin, D.B. Hibbert, *Anal. Commun.* 36 (1999) 225.
30. Y-D Zhao, W-D Zhang, H. Chen, Q-M Luo, *Analytical Sciences* 18 (2002) 939.
31. Y. Yin, Y. Lu, P. Wu, C. Cai, *Sensors.* 5 (2005) 220.
32. M. Wang, Y. Shen, Y. Liu, T. Wang, F. Zhao, B. Liu, S. Dong, *J. Electroanal. Chem*., 578 (2005) 121.
33. M.E.G. Lyons, *Sensors*. 2 (2002) 314.
34. A.J. Bard, L.R. Faulkner, *Electrochemical Methods*, Chapter 1, pp.14-18. Wiley, New York (2001).
35. N.S. Lawrence, R.P. Deo, J. Wang, *Electroanalysis* 17 (2005) 65.
36. (a) H.O. Finklea, L. Liu, M.S. Ravenscroft, S. Punturi, *J. Phys. Chem*., 100 (1996) 18852. (b) H.O. Finklea, *J. Electroanal. Chem*., 495 (2001) 79. (c) H.O. Finklea, K. Yoon, E. Chamberlain, J. Allen, R. Haddox, *J. Phys. Chem. B,* 105 (2001) 3088.

37. (a) C.E.D. Chidsey, *Science*. 251(1991) 919.(b) C.E.D. Chidsey, C.R. Bertozzi, T.M. Putvinski, A.M. Mujsce, *J. Am. Chem. Soc.* 112 (1990) 4301.
38. (a) C. Miller, P. Cuendet, M. Gratzel, *J. Phys. Chem*., 95 (1991) 877. (b) C. Miller, M. Gratzel, *J. Phys. Chem*., 95 (1991) 5225. (c) A.M. Becka, C.J. Miller, *J. Phys. Chem*., 96 (1992) 2657.
39. (a) R.J. Forster, L.R. Faulkner, *J. Am. Chem. Soc.,* 116 (1994) 5444. (b) R.J. Forster, L.R. Faulkner, *J. Am. Chem. Soc.,* 116 (1994) 5453. (c) R.J. Forster, J.P. O'Kelly, *J. Phys. Chem*., 100 (1996) 3695. (d) R.J. Forster, T.E. Keyes, *J. Phys. Chem. B.,* 105 (2001) 8829.
40. (a) L. Tender, M.T. Carter, R.W. Murray, *Anal. Chem*., 66 (1994) 3173. (b) G.K. Rowe, M.T. Carter, J.N. Richardson, R.W. Murray, *Langmuir*, 11 (1995) 1797.
41. M.J. Honeychurch, *Langmuir,* 14 (1998) 6291.
42. S.E. Creager, K. Weber, *Langmuir*, 9 (1993) 844.
43. See for example the excellent Wikipedia definition at http://en.wikipedia.org/wiki/Log-normal_distribution.
44. M.E.G. Lyons, G.P. Keeley, *Sensors*, 6 (2006) 1791.